Potentiation of cerebellar Purkinje cells facilitates whisker reflex adaptation through increased simple spike activity

Vincenzo Romano[1,5], Licia De Propris[1,2,5], Laurens W.J. Bosman[1,5,*], Pascal Warnaar[1], Michiel M. ten Brinke[1], Sander Lindeman[1], Chiheng Ju[1], Arthiha Velauthapillai[1], Jochen K. Spanke[1], Emily Middendorp Guerra[1], Tycho M. Hoogland[1,2], Mario Negrello[1], Egidio D'Angelo[3,4] and Chris I. De Zeeuw[1,2,*]

[1]Department of Neuroscience, Erasmus MC, Rotterdam, 3000 CA, the Netherlands

[2]Netherlands Institute for Neuroscience, Royal Academy of Arts and Sciences, Amsterdam, 1105 BA, the Netherlands

[3]Department of Brain and Behavioral Sciences, University of Pavia, Pavia, 27100, Italy

[4]Brain Connectivity Center, Instituto Fondazione C. Mondino, Pavia, 27100, Italy

[5]These authors contributed equally.

[*]Correspondence to: Chris I. De Zeeuw, Department of Neuroscience, PO Box 2040, 3000 CA Rotterdam, the Netherlands, c.dezeeuw@erasmusmc.nl or Laurens W.J. Bosman, Department of Neuroscience, PO Box 2040, 3000 CA Rotterdam, the Netherlands, l.bosman@erasmusmc.nl

Summary

Cerebellar plasticity underlies motor learning. However, how the cerebellum operates to enable learned changes in motor output is largely unknown. We developed a sensory-driven adaptation protocol for reflexive whisker protraction and recorded Purkinje cell activity from crus 1 and 2 of awake mice. Before training, simple spikes of individual Purkinje cells correlated during reflexive protraction with the whisker position without lead or lag. After training, simple spikes and whisker protractions were both enhanced with the spiking activity now leading the behavioral response. Neuronal and behavior changes did not occur in two cell-specific mouse models with impaired long-term potentiation at parallel fiber to Purkinje cell synapses. Consistent with cerebellar plasticity rules, increased simple spike activity was prominent in cells with low complex spike response probability. Thus, potentiation at parallel fiber to Purkinje cell synapses may contribute to reflex adaptation and enable expression of cerebellar learning through increases in simple spike activity.

Impact statement

Romano et al. show that expression of cerebellar whisker learning can be mediated by increases in simple spike activity, depending on LTP induction at parallel fiber to Purkinje cell synapses.

Introduction

Active touch is important for exploring our environment, allowing us to assess the shape, substance and movements of objects and organisms around us (Prescott et al., 2011). Throughout the animal kingdom, various systems have evolved for this purpose; these include for example the antennae of insects, the fingertips of primates and the well-developed whisker systems of rodents and sea mammals (Ahl, 1986, Dehnhardt et al., 2001, Staudacher et al., 2005, Dere et al., 2007, Anjum and Brecht, 2012). Activation of these sensory organs can provoke reactive movements, often occurring as a reflex (Nguyen and Kleinfeld, 2005, Bellavance et al., 2017, Brown and Raman, 2018, Staudacher et al., 2005). For survival it is important to maintain optimal control of such reflexes in daily life and to be able to adapt these movements (Voigts et al., 2015, Anjum and Brecht, 2012, Arkley et al., 2017).

Given the impact of cerebellar plasticity on a wide variety of motor learning tasks (Herzfeld et al., 2015, Herzfeld et al., 2018, Medina and Lisberger, 2008, Ten Brinke et al., 2015, Thier et al., 2002, Voges et al., 2017, Yang and Lisberger, 2017), it can be anticipated that adaptation of reflexive whisker movements is also partly controlled by plastic processes in the cerebellum. Historically, most studies on cerebellar learning have suggested that long-term depression (LTD) at the parallel fiber to Purkinje cell (PC) synapse may act as the main cellular mechanism underlying induction of cerebellar motor learning (Albus, 1971, Konnerth et al., 1992, Ito, 2003, Koekkoek et al., 2003, Medina and Lisberger, 2008, Boele et al., in press, Narain et al., 2018). However, parallel fiber LTD is unlikely to be the sole cellular mechanism underlying cerebellar learning (Gao et al., 2012, Hansel et al., 2001, D'Angelo et al., 2016). Short-term forms of plasticity probably also contribute, as some forms of behavioral adaptation can be linked to changes in PC activity during the previous trial (Yang and Lisberger, 2014, Herzfeld et al., 2018). Moreover, long-term potentiation (LTP) of

parallel fiber to PC synapses may also be relevant, as various PC-specific mutants with impaired LTP show deficits in cerebellar learning (Schonewille et al., 2010, Schonewille et al., 2011, Rahmati et al., 2014, Gutierrez-Castellanos et al., 2017). Possibly, different cerebellar cellular mechanisms dominate the induction of different forms of learning, dependent on the requirements of the downstream circuitries involved (De Zeeuw and Ten Brinke, 2015, Suvrathan et al., 2016).

While many studies have focused on the synaptic mechanism(s) that may induce cerebellar motor learning, the spiking mechanisms that are responsible for the expression thereof remain relatively unexplored. To date, whereas evidence is emerging that the expression of conditioned eyeblink responses is mediated by a long-lasting *suppression* of simple spikes of PCs in the deep fissure of lobule simplex (Heiney et al., 2014, Halverson et al., 2015, Ten Brinke et al., 2015), it is unclear to what extent enduring *increases* in simple spike activity can also contribute to the expression of cerebellar learning, and if so for what forms of learning. Here, we developed a novel whisker training paradigm that is likely to generate plasticity in the cerebellar cortex and to produce increases in simple spike activity at the PC level following induction of LTP at the parallel fiber to PC synapse (D'Angelo et al., 2001, Lev-Ram et al., 2002, Lev-Ram et al., 2003, Coesmans et al., 2004, Ramakrishnan et al., 2016, van Beugen et al., 2013). Indeed, we show that a brief period of 4 Hz air-puff stimulation of the whiskers can enhance touch-induced whisker protraction as well as PC simple spike firing for tens of minutes. Moreover, these behavioral and neuronal changes are both absent in two independent mouse mutant lines deficient for parallel fiber to PC LTP, bridging the putative mechanism of memory expression with that of memory induction.

Results

Touch-induced whisker protraction

The large facial whiskers are a prime source of sensory information for many mammals, in particular for rodents that can make elaborate movements with their large facial whiskers (Arkley et al., 2017, Brecht, 2007, Welker, 1964, Bosman et al., 2011, Vincent, 1913). It has been noted that passive touch can trigger active whisker movements in mice (Bellavance et al., 2017, Brown and Raman, 2018, Nguyen and Kleinfeld, 2005, Ferezou et al., 2007), but this behavior has not been described in great detail yet. Here, we studied whisker movements following rostro-caudal air-puff stimulation of the whisker pad in 16 awake, head-restrained mice (Figure 1A-C). The air-puffer was placed in such a way that most, if not all, large mystacial whiskers were affected by the air flow from the front. The mice made active whisker protractions following the largely passive retractions induced by the air flow in the large majority (82%) of stimulus trials (Figure 1D-E; Figure 1 – figure supplement 1C). Because of the systematic full-field air-flow from the front, the touch-induced protraction was typically performed by all whiskers simultaneously (*data not shown*), which is in line with the presumed reflexive nature of this movement (Bellavance et al., 2017, Brown and Raman, 2018, Nguyen and Kleinfeld, 2005). Moreover, as reported previously (Ferezou et al., 2007), the touch-induced whisker protraction was followed in about half the trials (51%) by extended periods of active whisker movements during the subsequent 200 ms interval (Figure 1D; Figure 1 – figure supplement 1A-C). However, under our experimental conditions with a 2 s inter-trial interval, spontaneous whisking in between the stimuli was relatively rare. Across all 16 mice measured, we found spontaneous movements (with an amplitude exceeding 10°) only in 12% of the 100 trials per mouse during the 200 ms interval prior to stimulus onset.

To find out whether touch-induced whisker protraction can indeed be described as a reflex (Bellavance et al., 2017, Brown and Raman, 2018, Nguyen and Kleinfeld, 2005), we wanted to know to what extent the movements also show signs characteristic of startle responses or voluntary events, which have a different identity. A startle response would be expected to be not only highly stereotypic, but to also show relatively little direction-specificity, and to reveal signs of pre-pulse inhibition (Gogan, 1970, Swerdlow et al., 1992, Moreno-Paublete et al., 2017). Instead, if the air-puff triggered a conscious, explorative movement, the animal would most likely make spontaneous movements towards the source of the air-puff, dependent on its specific position. To explore these possibilities, we placed a second air-puffer at the caudal side of the whisker field and a third air-puffer at the front of the contralateral whisker field, and we provided air-puffs from the three different orientations, intermingling trials with and without brief pre-pulses in random order (Figure 1 – figure supplement 2A). An air-puff from the front on the ipsilateral side induced a largely passive retraction prior to the active protraction. Such a retraction was mostly absent when stimulating from the back. Contralateral stimulation also evoked a slight retraction, followed by a much larger forward sweep (Figure 1 – figure supplement 2B-E; Table S1). Thus, applying the air-puff from different angles produced different retractions and different subsequent protractions, arguing against a stereotypical startle behavior that occurs independent from the stimulus conditions. Moreover, we did not observe a diminishing effect of the weaker pre-pulse on the reaction to the stronger pulse ($p = 0.268$; Dunn's pairwise post-hoc test after Friedman's ANOVA; $p = 0.003$; Fr = 13.933; df = 3). Finally, we also did not observe distinct explorative movements linked to the puff sources, which might have suggested dominant voluntary components (Figure 1 - figure supplement 2B-C). Altogether, the reactive nature of the touch-induced whisker movements in the absence of characteristic

signs of startle or voluntary responses indicates that the air-puff induced protraction is indeed a reflexive movement.

Anatomical distribution of Purkinje cell responses to whisker pad stimulation

In line with the fact that PCs receive sensory whisker input not only directly from the brainstem but also indirectly from thalamo-cortical pathways (Figure 2F) (Kleinfeld et al., 1999, McElvain et al., 2018, Bosman et al., 2011, Brown and Raman, 2018, Kubo et al., 2018), the dynamics of their responses upon whisker stimulation are heterogeneous (Brown and Bower, 2001, Loewenstein et al., 2005, Bosman et al., 2010, Chu et al., 2011). To study the anatomical distribution of these responses within cerebellar lobules crus 1 and crus 2 we mapped the complex spike and simple spike firing of their PCs following ipsilateral whisker pad stimulation with air-puffs in awake mice. Of the 132 single-unit PCs from which we recorded, 118 (89%) showed significant complex spike responses, albeit with large variations in latency and amplitude (Figure 2A-C, Figure 2 – figure supplement 1A-B). We considered a response to be significant if it passed the threshold of 3 s.d. above the average of the pre-stimulus interval. Cluster analysis revealed that in terms of complex spike modulation PCs can better be considered as two separate clusters rather than a continuum spectrum (indicated by the lowest absolute BIC value for two components (437, compared to 490 and 442 for one and three components, respectively; Figure 2 – figure supplement 1D). We refer to the cells of the cluster with the higher complex spike response probability as "strong" (34%, with a peak response above 1.98%; see Methods) and the other as "weak" (66%) responders (Figure 2 – figure supplement 1D-F). Similarly, of the 132 recorded PCs 127 (96%) showed a significant simple spike response. Simple spike responses were often bi-phasic, consisting of a period of inhibition followed by one of excitation, or vice versa (Figure 2D-E, Figure 2 – figure supplement 1C). The trough of the simple spike responses typically correlated in a

reciprocal fashion with the peak of the complex spike responses (Figure 2A-E; Figure 2 – figure supplement 1A-C) (De Zeeuw et al., 2011, Zhou et al., 2014, Badura et al., 2013). Only 2 PCs, out of the 132, did not show any significant modulation (i.e. for neither complex spikes nor simple spikes). To chart the spatial distribution of the PCs with different response kinetics upon whisker stimulation we first combined electrolytic lesions (Figure 2G) with reconstructions of the electrode entry points, generating a map of the locations of the PCs from which we recorded with the quartz/platinum electrodes (n = 132). Complex spike responses to whisker stimulation were found to be especially strong in parts of crus 1 overlapping with large areas of the C2, D1 and D2 zones (Figure 2H), whereas the primary simple spike responses were predominantly facilitating in adjacent areas in the medial and lateral parts of crus 1 and crus 2, as predicted by the overall tendency for reciprocity (Figure 2H-I; Figure 2 – figure supplement 1G-H). This distribution was verified using double-barrel glass pipettes with which we injected the neural tracer, BDA 3000, at the recording spot after recording complex spike responses. Following identification of the source of the climbing fibers in the inferior olive and the projection area in the cerebellar nuclei (Figure 2 – figure supplement 2A-C), we defined the cerebellar area in which the recorded PC was located (Apps and Hawkes, 2009, Voogd and Glickstein, 1998). These experiments confirmed that the PCs with strong complex spike responses were situated most prominently in centro-lateral parts of crus 1, whereas the PCs with weak complex spike responses were predominant in adjacent areas in crus 1 and crus 2 (Figure 2 – figure supplement 2D).

Large reflexive whisker protractions are preceded by complex spikes

As complex spikes have been reported to be able to encode, at the start of a movement, the destination of arm movements (Kitazawa et al., 1998), we wondered whether a similar association could be found for whisker movements. Therefore, we asked whether trials that

started with a complex spike involved larger or smaller protractions. To this end, we separated all trials of a session based upon the presence or absence of a complex spike during the first 100 ms after stimulus onset in a single PC. It turned out that during the trials with a complex spike, the protraction was significantly larger (see Figure 3A for a single PC; Figure 3B for the population of 55 PCs of which we had electrophysiological recordings during whisker tracking and that responded to air-puff stimulation). A direct comparison between the timing of the complex spike response and the difference in whisker position between trials with and without a complex spike revealed that the peak in complex spike activity preceded the moment of maximal difference in position by 63 ± 4 ms (mean ± SEM; $n = 55$; Figure 3C-D). The maximal difference in protraction in trials with a complex spike equaled 0.80° (median, with IQR of 2.80°; $p < 0.001$), whereas this was only 0.28° (0.92°) for retraction ($p = 0.002$; Wilcoxon matched pairs tests, significant after Bonferroni correction for multiple comparisons: $\alpha = 0.05/3 = 0.017$) (Figure 3E). These findings imply that trials that started with a complex spike showed bigger whisker protractions than those without a complex spike.

We next questioned whether there was a correlation between the strength of the complex spike response and the difference in maximal protraction. This did not seem to be the case (R = 0.119; $p = 0.386$; Pearson correlation; Figure 3 – figure supplement 1A). Thus, in general, the complex spike of any PC showing whisker-related complex spike activity could have a similar predictive power for the amplitude of the subsequent protraction. In line with this, a map showing the distribution of the PCs based upon the correlation of their complex spikes with whisker protraction was fairly homogeneous. Only in an area overlapping with the rostral part of crus 1, a small cluster of PCs was observed whose complex spikes correlated with an unusually large difference in protraction (Figure 3 – figure supplement 1B). However, since sensory-induced complex spikes were typically more frequent in lateral crus 1, PCs in

this area appeared to have overall a stronger correlation with increased touch-induced whisker protraction than the PCs in the surrounding areas (Figure 3 – figure supplement 1C).

Previous studies showed that motor control can be related to the coherence of complex spike firing of adjacent PCs (Mukamel et al., 2009, Hoogland et al., 2015). We therefore expected to observe also increased coherence at the trial onsets in our experiments. To test this, we performed two-photon Ca^{2+} imaging to study the behavior of adjacent groups of PCs in crus 1 around the moment of whisker pad air-puff stimulation in awake mice. After injection of the Ca^{2+}-sensitive dye Cal-520 we could recognize the dendrites of PCs as parasagittal stripes, each of which showed fluorescent transients at irregular intervals (Figure 3 – figure supplement 2A-B). Previous studies identified these transients as the result of PC complex spike firing (Ozden et al., 2008, Tsutsumi et al., 2015, Schultz et al., 2009, De Gruijl et al., 2014). Occasionally, signals could be found that were shared by many PCs, even in the absence of sensory stimulation (Figure 3 – figure supplement 2B) in line with earlier reports (Ozden et al., 2009, De Gruijl et al., 2014, Mukamel et al., 2009, Schultz et al., 2009). Upon whisker pad stimulation, however, complex spike firing occurred much more often collectively in multiple Purkinje cells (Figure 3 – figure supplement 2C). To quantify this form of coherent firing, we counted the number of complex spikes fired per frame (of 40 ms) and determined the level of coherence using cross-correlation analyses (Figure 3 – figure supplement 2D) (see also Ju et al., (2018)). The levels of coherence increased to such strength that they were extremely unlikely to have occurred by the increase in firing frequency alone (compared to a re-distribution of all events based on a Poisson distribution; Figure 3 – figure supplement 2E). In other words, firing of a single or a few PCs was the dominant mode of activity in the absence of stimulation, and this changed towards the involvement of multiple PCs upon stimulation, firing coherently as can be seen in the change in distribution of coherently active PCs (Figure 3 – figure supplement 2F-G). We conclude that groups of

adjacent PCs respond to whisker pad stimulation by increased complex spike firing with an enhanced level of coherence, which is likely to further facilitate the occurrence of bigger whisker reflexes (see above).

Instantaneous simple spike firing correlates with whisker protraction during reflex

The firing rate of simple spikes has been shown to correlate with whisker position: in the large majority of PCs, simple spike firing is correlated with protraction and in a minority it correlates with retraction (Brown and Raman, 2018, Chen et al., 2016). This led us to study the correlation in simple spike firing during touch-induced whisker protraction. At first sight, variation in simple spike firing roughly correlated to periods with whisker movement (Figure 4A-B). To study this in more detail, we made use of the inter-trial variations in simple spike rate and whisker position, allowing us to make a correlation matrix between these two variables on a trial-by-trial basis (see Ten Brinke et al., (2015)). In a representative example (Figure 4C), the whisker protraction and peak in simple spike firing were roughly simultaneous. In the correlation matrix, this is visualized by the yellow color along the 45° line. This turned out to be the general pattern in 25 of the 56 PCs (45%) of which we had electrophysiological recordings during whisker tracking (Figure 4D). In all of these 25 PCs, there was a positive correlation between instantaneous simple spike firing and whisker protraction that occurred relatively late during the movement, in particular between 80 and 200 ms after the start of the stimulus (Figure 4C-D; Figure 4 – figure supplement 1A-C), thus well after the complex spike responses occurred (Figure 3C). In the 31 remaining PCs, i.e. the ones that did not display a significant correlation when evaluated at the level of individual cells, we still observed a slight, yet significant, correlation at the population level. Remarkably, this correlation was slightly negative, i.e. possibly reflecting a correlation between simple spike firing and retraction (Figure 4 – figure supplement 1). We conclude that

during the touch-induced whisker reflex simple spikes predominantly correlate with whisker protraction and that this correlation is maximal without a clear time lead or lag, unlike the complex spikes, the occurrence of which tended to precede the reflexive protraction.

4 Hz air-puff stimulation leads to acceleration of simple spike response and to stronger protraction of whiskers

Next, we investigated whether sensory experience could modulate the touch-induced whisker protraction, the frequency of simple spike firing and the relation between them. We hypothesized that whisker movements might be enhanced following air-puff stimulation at 4 Hz, as this frequency has been shown to be particularly effective in inducing potentiation at the parallel fiber-to-PC synapse (Coesmans et al., 2004, D'Angelo et al., 2001, Lev-Ram et al., 2002, Ramakrishnan et al., 2016). Indeed, application of this 4 Hz air-puff stimulation to the whisker pad for only 20 seconds was sufficient to induce an increase in the maximal protraction (average increase 17.9 ± 3.9%; mean ± SEM; $p < 0.001$; Wilcoxon-matched pairs test; $n = 16$ mice) (Figure 5A-B; Table S2).

This change in the amplitude of the touch-induced whisker protraction was not accompanied by any substantial change in the complex spike response to whisker pad stimulation ($p = 0.163$; Wilcoxon matched pairs test; $n = 55$ PCs) (Figure 5C; Table S2). However, the rate of simple spike firing upon air-puff stimulation was markedly increased after 20 s of 4 Hz air-puff stimulation. This was especially clear during the first 60 ms after the air-puff ($p = 0.003$; Wilcoxon matched pairs test; $n = 55$ PCs) (Figure 5D; Table S2). Overlaying the averaged whisker traces and PC activity profiles highlighted the earlier occurrence of facilitation in simple spike firing after the 4 Hz air-puff stimulation protocol (Figure 5E). To study this timing effect in more detail, we repeated the trial-based correlation analysis (cf. Figure 4C-D). The short period of 4 Hz air-puff stimulation caused an

anticipation of the moment of maximal correlation between simple spike firing and whisker position. Along the 45° line – thus regarding only the zero-lag correlation between simple spike firing and whisker position – this changed from 152.1 ± 18.1 ms to 90.7 ± 9.4 ms (means ± SEM); p = 0.020; t = 2.664; df = 13; paired t test; n = 14 PCs) (Figure 5 – figure supplement 1A-B). The slope of the correlation between the instantaneous simple spike frequency and the whisker position remained unaltered (p = 0.197, t = 1.360, df = 13, n = 14, paired t test) (Figure 5 – figure supplement 1C-D). However, the point of maximal correlation was no longer with a zero-lag, but after induction the simple spikes led the whisker position (pre-induction: Δtime = 0 ± 10 ms; post-induction: Δtime = 20 ± 30 ms; medians ± IQR; n = 14; p = 0.001; Wilcoxon matched-pairs test) (Figure 5F). Thus, not only the simple spike rate increased, but also its relative timing to the touch-induced whisker protraction, now preceding the likewise increased touch-induced whisker protraction.

During the entrainment itself (i.e., during the 20 s period with 4 Hz air-puff stimulation), the whisker responses as well as the complex spike and the simple spike responses to each air-puff were weakened compared to the pre-induction period during which we used 0.5 Hz stimulation. More specifically, the touch-induced whisker protraction decreased by 62.2% (median; IQR = 37.5%); the maximum response of the complex spikes significantly decreased from a median of 1.27% (with an IQR of 1.89%) during pre-induction to 0.52% (with an IQR of 0.43%) during induction (p < 0.001; Wilcoxon matched pairs tests, n = 55 PCs); and the average modulation of the simple spikes in the first 200 ms after the puff decreased from a median of 5.9% (with an IQR of 18.2%) during pre-induction to -0.3% (IQR = 3.13) during induction (p = 0.039, Wilcoxon matched-pairs test) (Figure 5 – figure supplement 2). Thus, during the 4 Hz training stage, all responses – both at the behavioral and neuronal level – diminished compared to the preceding 0.5 Hz stimulation stage.

Given the correlation between instantaneous simple spike rate and whisker position described above, one would expect that contralateral air-puff stimulation – which triggers a stronger protraction (Figure 1 – figure supplement 2) – also triggers a stronger simple spike response. To test this hypothesis we recorded PC activity while stimulating the ipsi- and contralateral whiskers in a random sequence (Figure 5 – figure supplement 3A-B). The change in maximal protraction was considerable (difference in maximal protraction: 7.30 ± 1.24° (mean ± SEM); n = 9 mice) (Figure 5 – figure supplement 3C; cf. Figure 1 – figure supplement 2E). Possibly, the absence of the direct mechanical retraction on the ipsilateral side during contralateral air-puff stimulation can explain part of this difference, which is also in line with the earlier onset of the protraction during contralateral stimulation (Figure 5 – figure supplement 3C). However, in addition to this passive process, a change in simple spikes may contribute to this difference as well, as the simple spikes increased significantly more during contralateral stimulation (increase during first 60 ms after air-puff onset for contra- vs. ipsilateral stimulation: 13.7 ± 5.3%; mean ± SEM; p = 0.023; t = 2.413; df = 26; paired t test; n = 27 PCs) (Figure 5 – figure supplement 3E). Such a contribution is compatible with the fact that most mossy fiber pathways related to whisker movement are bilateral with a contralateral preponderance (Bosman et al., 2011). Instead, the complex spikes were less activated during contralateral stimulation (complex spike peak response: ipsilateral: 1.40% (1.25%); contralateral: 0.71% (0.81%); medians (IQR); $p < 0.001$; Wilcoxon matched-pairs test; n = 27 PCs) (Figure 5 – figure supplement 3D). This response is in line with a bilateral component of the projection from the trigeminal nucleus to the olive (De Zeeuw et al., 1996).

To establish a causal link between increases in simple spike firing and whisker protraction, artificial PC stimulation would also have to affect whisker movement. Previously, it has been shown that simple spikes modulate ongoing whisker movements rather than initiate them (Brown and Raman, 2018, Chen et al., 2016, Proville et al., 2014). To find out

whether simple spike firing could modulate touch-induced whisker protraction under our recording conditions, we investigated the impact of activation of PCs by optogenetic stimulation. To this end we used L7-Ai27 mice, which express channelrhodopsin-2 exclusively in their PCs and which respond with a strong increase in their simple spike firing upon stimulation with blue light (Witter et al., 2013). We placed an optic fiber with a diameter of 400 µm over the border between crus 1 and crus 2 and compared air-puff induced whisker movements among randomly intermingled trials with and without optogenetic PC stimulation. The period of optogenetic stimulation (i.e. 100 ms) was chosen to mimic preparatory activity of PCs and thus corresponded well to the period during which we observed increased simple spike firing after 4 Hz air-puff stimulation (Figure 5D). As expected, the whisker protraction was substantially bigger during the period of optogenetic stimulation ($p < 0.001$; $t = 4.411$; df = 12; paired t test; n = 13 mice; Figure 5 – figure supplement 4). Thus, even though optogenetic stimulation of PCs can also trigger secondary feedback mechanisms that may influence the outcome (Witter et al., 2013, Chaumont et al., 2013), we conclude that increases in simple spike firing can cause stronger whisker protraction.

Complex spikes inhibit increased simple spike firing

As cerebellar plasticity is bi-directional and under control of climbing fiber activity (Ohtsuki et al., 2009, Lev-Ram et al., 2003, Coesmans et al., 2004), we wanted to find out to what extent plastic changes in simple spike activity can be related to the strength of the complex spike response generated by climbing fibers. To this end we compared for each PC the strengths of the complex spike and simple spike responses before, during and after the 4 Hz air-puff stimulation. As expected, we found a significant negative correlation between the strength of the complex spike response, as measured by the peak of the PSTH before the 4 Hz air-puff stimulation, and the change in simple spike response following this 4 Hz stimulation

(R = 0.311; p = 0.021; Pearson correlation n = 55 PCs) (Figure 6A). We further substantiated these findings by looking separately at the average complex spike firing frequency of the strong and weak responders (cf. Figure 2 – figure supplement 1E). The correlation found between the frequency of complex spike firing and the change in simple spike activity after 4 Hz air-puff stimulation proved to be present only in the weak responders, taking the firing rate during the pre-induction and induction period into account (Figure 6 – figure supplement 1). This is again in line with the notion that parallel fiber activity in the absence of climbing fiber activity promotes parallel fiber to PC LTP (Coesmans et al., 2004, Lev-Ram et al., 2002, Ramakrishnan et al., 2016). The PCs with the strongest effect of 4 Hz air-puff stimulation on simple spike firing were mainly located in the lateral part of crus 2 (Figure 6B), posterior to the crus 1 area with the strongest complex spike responses (Figure 2H). We compared the location of this lateral crus 2 area to that of the PCs with the strongest correlations between simple spike firing and whisker protraction and we found these two crus 2 locations to match well (Figure 6B-C).

The impact of 4 Hz air-puff stimulation on the simple spike activity of PCs with a weak complex spike response lasted as long as our recordings lasted (i.e. at least 30 min), whereas that on PCs with a strong complex spike response was not detectable during this period (Figure 6D-F). Indeed, the weak responders differed significantly from the strong responders in this respect (weak vs. strong responders: p = 0.005; F = 3.961; df = 4.424; two-way repeated measures ANOVA with Greenhouse-Geyser correction; n = 8 weak and n = 6 strong responders; Fig. 6F). Likewise, the impact of the 4 Hz air-puff stimulation on touch-induced whisker protraction also lasted throughout the recording in that the protraction sustained (Figure 6 – Figure supplement 2). Thus, both simple spikes and whisker muscles remained affected by the 4 Hz air-puff stimulation for as long as our recordings lasted.

Expression of PP2B in Purkinje cells is required for increased protraction and simple spike firing following 4 Hz air-puff stimulation

In reduced preparations, 4 Hz stimulation of the parallel fiber inputs leads to LTP of parallel fiber to PC synapses (Coesmans et al., 2004, Lev-Ram et al., 2002, Ramakrishnan et al., 2016). At the same time, parallel fiber LTP is inhibited by climbing fiber activity (Coesmans et al., 2004, Lev-Ram et al., 2003, Ohtsuki et al., 2009). Hence, our data appear in line with a role for parallel fiber LTP as a potential mechanism underlying the observed increase in simple spike firing upon a brief period of 4 Hz stimulation. To further test a potential role for LTP, we repeated our 4 Hz air-puff stimulation experiments in L7-PP2B mice, which lack the PP2B protein specifically in their PCs, rendering them deficient of parallel fiber-to-PC LTP (Schonewille et al., 2010) (Figure 7A). The impact of 4 Hz air-puff stimulation on the maximal protraction was significantly less in the L7-PP2B mutant mice compared to wild types ($p = 0.044$, $t = 2.162$, df = 19, *t* test; Figure 7B-D). Accordingly, in contrast to those in their wild type (WT) littermates ($p < 0.001$, $t = 4.122$, df = 15, *t* test), the maximal touch-induced whisker protraction before and after induction was not significantly different in L7-PP2B mice ($p = 0.647$, $t = 0.470$, df = 12, *t* test; Fig. 7E). Thus, L7-PP2B mice do not show increased touch-induced whisker protraction after 4 Hz air-puff stimulation.

In line with the absence of increased touch-induced whisker protraction, also the increase in simple spike firing observed in wild type mice was absent in L7-PP2B mice. As the strong complex spike responders in WTs did not show changes in simple spike activity (cf. Figure 6), we compared weak complex spike responders of both genotypes. Simple spike responses were stably increased in WT PCs with a weak complex spike response following 4 Hz air-puff stimulation (as shown in Figure 6F), but not in those of L7-PP2B mice (effect of genotype: $p = 0.003$, $F = 4.361$, df = 4.137, two-way repeated measures ANOVA with Greenhouse-Geyser correction; $n = 8$ WT and $n = 9$ L7-PP2B PCs) (Figure 7F). Despite the

lack of potentiation, we found that the L7-PP2B mice still had a significant correlation between the complex spike frequency during the induction block and changes in simple spike activity (R = 0.489, p = 0.013, Pearson correlation; Figure 7 – figure supplement 1A); this correlation may result from other forms of plasticity that are still intact in L7-PP2B mice (Schonewille et al., 2010). Yet, in line with the absence of increased simple spike responsiveness, the correlation between changes in simple spike firing during the induction block and the impact of 4 Hz air-puff stimulation, as present in the WT PCs, was absent in the L7-PP2B mice (Figure 7 - figure supplement 1B). Thus, in the absence of the PP2B protein in PCs, the impact of 4 Hz air-puff stimulation on touch-induced whisker protraction as well as on the simple spike responsiveness was not detectable. These correlations between complex spike and simple spike firing on the one hand and modification of the simple spike response to whisker pad stimulation on the other hand further strengthen our hypothesis that parallel fiber to PC LTP is one of the main mechanisms that underlies the long-term changes that can be observed at both the level of simple spike activity and whisker protraction after 4 Hz air-puff stimulation.

Expression of AMPA receptor GluA3 subunits in Purkinje cells is required for increased protraction and simple spike firing following 4 Hz air-puff stimulation

To control for compensatory mechanisms specific for L7-PP2B mice we used a second, independent, yet also PC-specific, mutant mouse line deficient in parallel fiber LTP. In these mice (L7-GluA3), PCs lack the GluA3 subunit (Gutierrez-Castellanos et al., 2017). As in the L7-PP2B mice, we did not find evidence for increased whisker protraction after 4 Hz air-puff stimulation (e.g., change in whisker angle during the first 120 ms after air-puff onset: WT vs. L7-GluA3 mice: p = 0.007, Tukey's post-hoc test after ANOVA (p = 0.001, F = 9.111, df = 2), n = 16 WT and n = 6 GluA3 deficient mice) (Figure 8A-C). Moreover, as in the L7-PP2B

412 mice, also the increase in simple spike responsiveness after 4 Hz stimulation was absent in
413 L7-GluA3 mice (change in simple spike count between WT and L7-GluA3 PCs during the
414 first 60 ms after air-puff onset: $p = 0.004$; Tukey's post-hoc test after ANOVA ($p = 0.002$, $F =$
415 6.681, df = 2), $n = 35$ WT PCs and $n = 13$ GluA3 KO PCs, next to $n = 23$ L7-PP2B KO PCs,
416 all with weak complex spike responses) (Figure 8D-F). Thus an independent line of evidence
417 supports the findings made in the L7-PP2B mice.

418 For control we compared the basic electrophysiological profiles of PCs in the three
419 genotypes used in this study. When averaged over the entire period with episodes of
420 stimulation, the overall complex spike rate, simple spike rate and simple spike CV2 value (i.e.
421 parameter for level of irregularity) of PCs in the L7-PP2B KO mice were moderately, but
422 significantly, reduced compared to those in WTs (Figure 8 – figure supplement 1A-D; Table
423 S3). However, as the L7-GluA3 mice did not show any significant deviations in these overall
424 firing properties (Figure 8 – figure supplement 1A-D; Table S3), it is unlikely that the
425 aberrant firing properties of L7-PP2B mice could explain the lack of adaptation at both the
426 behavioral and electrophysiological level. Comparing the response probabilities to whisker
427 pad stimulation we found that both the number of complex spikes and simple spikes after the
428 air-puff were reduced in L7-PP2B mice (Figure 8 – figure supplement 1E-J; Table S3). The
429 predominantly suppressive simple spike responses were not found in L7-GluA3 mice, but the
430 latter also had a reduced complex spike response to air-puff stimulation. Since a reduced
431 complex spike response acts permissive for the adaptive increase in the simple spike response,
432 it is unlikely that the observed reduction in complex spike firing would be the cause of the
433 observed lack of simple spike enhancement in both mutant mouse lines. Moreover, the
434 amplitudes of the touch-induced whisker protraction as measured before the induction phase
435 were similar between the WT and the mutant mice (Figure 8 – figure supplement 2). We
436 therefore conclude that the absence of simple spike potentiation and the concomitant increase

437 in touch-induced whisker protraction is likely due to the absence of parallel fiber LTP caused

438 by the genetic mutations rather than to altered firing patterns of the PCs involved.

Discussion

In this study we show for the first time that a brief period of intense sensory stimulation can evoke adaptation of reflexive whisker protraction. Extracellular recordings revealed that the simple spike activity of the PCs that modulate during whisker movements is congruently increased when the adapted behavior is expressed. These PCs, which are predominantly located in the crus 2 region, show a present but weak complex spike response to whisker stimulation, which appears to act permissive for the occurrence of parallel fiber to PC LTP. This form of plasticity is likely to be one of the main mechanisms underlying this whisker reflex adaptation, as two independent cell-specific mouse models, both of which lack LTP induction at their parallel fiber to PC synapses, did not show any alteration in their whisker protraction or simple spike response following the training protocol with 4 Hz air-puff stimulation. By contrast, the PCs that show a strong complex spike response to whisker stimulation and that are mainly located in crus 1 did not manifest a prominent regulatory role to enhance the simple spike responses or whisker movements in the long-term. Our study highlights how moderate climbing fiber activity may permit induction of PC LTP in a behaviorally relevant context and how this induction may lead to an increase in simple spike modulation when the adapted motor output is expressed.

Control of whisker movements

Although most mammals have whiskers, only few species use their whiskers to actively explore their environment by making fast, rhythmic whisker movements (Vincent, 1913, Ahl, 1986, Welker, 1964, Woolsey et al., 1975). In “whisking” animals, such as mice and rats, whisker protraction is under direct muscle control, while whisker retraction is largely mediated by a passive process involving skin elasticity (Berg and Kleinfeld, 2003, Simony et

al., 2010, Haidarliu et al., 2015). Animals can modify the pattern of whisker movements upon sensory feedback during natural behavior, as has been demonstrated for example during gap crossing and prey capture (Anjum and Brecht, 2012, Voigts et al., 2015). The neural control of adaptation of reflexive whisker movements is still largely unknown. Given the widespread networks in the brain controlling whisker movements (Bosman et al., 2011, Kleinfeld et al., 1999), it is likely that multiple brain regions contribute. We show here, at least for a specific reproducible form of whisker adaptation, that parallel fiber to PC LTP and enhancement in PC simple spike activity may contribute to the induction and expression of this form of motor learning, respectively.

Simple spike firing during normal and adapted whisker movements

Our electrophysiological recordings indicate that the simple spike activity correlates well with whisker protraction, especially in PCs located in crus 2, and that this relation is context-dependent. Under the baseline condition of our paradigm, during the 0.5 Hz whisker pad stimulation, simple spikes correlate positively with the position of the whiskers during protraction on a single trial basis. The correlation between the rate of simple spikes and that of protraction was also found when comparing the impact of contralateral vs. ipsilateral whisker pad stimulation. The absence of a clear time lag or lead between simple spike activity and whisker movements under this condition suggests that during normal motor performance without sensorimotor mismatch signaling the simple spikes predominantly represent ongoing movement. Our data under baseline conditions are compatible with those obtained by the labs of Chadderton and Léna (Chen et al., 2016, Proville et al., 2014). In their studies on online motor performance, the simple spike activity of most PCs in the lateral crus 1 and/or crus 2 regions correlated best with protraction of the set point, defined as the slowly varying midpoint between maximal protraction and maximal retraction.

During and after training with 4 Hz air-puff stimulation the temporal dynamics of the simple spikes shifted in that the simple spikes were found to precede the whisker movement and to predict the magnitude of the protraction, suggesting the emergence of an instructive motor signal. Optogenetic stimulation experiments confirmed that increased simple spike firing during the early phase of touch-induced whisker protraction can promote whisker protraction. Thus, the current dataset confirms and expands on previous studies, highlighting a role of the cerebellar PCs injecting additional accelerating and amplifying signals into the cerebellar nuclei during entrainment (De Zeeuw et al., 1995).

Cerebellar plasticity

Synaptic plasticity in the cerebellar cortex has, next to that in the cerebellar and vestibular nuclei (Lisberger and Miles, 1980, Lisberger, 1998, Zhang and Linden, 2006, McElvain et al., 2010), generally been recognized as one of the major mechanisms underlying motor learning (Ito, 2001, Ito, 2003). For forms of motor learning that require a decrease in simple spike activity for expression of the memory, such as eyeblink conditioning (Halverson et al., 2015, Ten Brinke et al., 2015, Jirenhed et al., 2007), long-term depression (LTD) of the parallel fiber to PC synapse may play a role during the initial induction stage (Ito, 2003, Koekkoek et al., 2003). In LTD-deficient mouse models the potential contribution of LTD is most apparent when compensatory mechanisms that involve activation of the molecular layer interneurons are blocked (Boele et al., in press). However, for forms of motor learning that require an increase in simple spike activity for expression of the procedural memory it is less clear which forms of cerebellar cortical plasticity may contribute. Here, we show that increasing whisker protraction by repetitive sensory stimulation requires an increase in simple spike activity and that blocking induction of parallel fiber to PC LTP prevents changes in both spiking and motor activity following the same training paradigm. Possibly, adaptation of the vestibulo-

ocular reflex (VOR) follows the same learning rules in that various genetic mouse models with impaired induction of parallel fiber to PC LTP show reduced VOR learning (Gutierrez-Castellanos et al., 2017, Rahmati et al., 2014, Schonewille et al., 2010, Ly et al., 2013, Peter et al., 2016) and that optogenetic stimulation of PCs in the flocculus of the vestibulocerebellum can increase VOR gain (Voges et al., 2017). In this respect it will be interesting to find out to what extent increases in simple spike activity in the flocculus can also be correlated with an entrained increase in VOR gain on a trial-by-trial basis, as we show here for whisker learning.

The differential learning rules highlighted above indicate that different forms of cerebellar plasticity may dominate the induction of different forms of learning (Hansel et al., 2001, Gao et al., 2012, D'Angelo et al., 2016, De Zeeuw and Ten Brinke, 2015). The engagement of these rules may depend on the requirements of the downstream circuitries involved (Suvrathan et al., 2016, De Zeeuw and Ten Brinke, 2015). Indeed, whereas the eyeblink circuitry downstream of the cerebellar nuclei comprises purely excitatory connections and hence requires a simple spike suppression of the inhibitory PCs to mediate closure of the eyelids, the VOR circuitry comprises an additional inhibitory connection and hence requires a simple spike enhancement so as to increase the compensatory eye movement (De Zeeuw and Ten Brinke, 2015, Voges et al., 2017). The circuitry downstream of the cerebellum that mediates control of whisker movements is complex (Bosman et al., 2011). Possibly, the cerebellar nuclei may modulate the trigemino-facial feedback loop in the brainstem that controls the touch-induced whisker protraction (Bellavance et al., 2017). This could be done via the intermediate reticular formation, which receives a direct input from the cerebellar nuclei (Teune et al., 2000) and projects to the facial nucleus where the whisker motor neurons reside (Zerari-Mailly et al., 2001, Herfst and Brecht, 2008). As the latter projection is inhibitory (Deschênes et al., 2016), the same configuration may hold as

539 described for the VOR pathways (De Zeeuw and Ten Brinke, 2015) in that adaptive
540 enhancement of the whisker reflex may require induction of parallel fiber to PC LTP and
541 increases in simple spike activity. Thus, given the current findings and the known neuro-
542 anatomical connections in the brainstem, the picture emerges that cerebellar control of
543 whisker movements follows the general pattern which suggests that the predominant forms of
544 PC plasticity and concomitant changes in simple spike activity align with the requirements
545 downstream in the cerebellar circuitry (De Zeeuw and Ten Brinke, 2015).
546
547 *Heterogeneous pools of PCs with differential complex spike responses to whisker stimulation*
548 A minority of the PCs we recorded had a high complex spike response probability upon air-
549 puff stimulation of the whisker pad. These PCs were predominantly located in the centro-
550 lateral part of crus 1. Most of the other PCs, in particular those in the medial part of crus 1 and
551 in crus 2, showed a low, yet significant, complex spike response probability to sensory
552 whisker stimulation. In these cells the absence of a strong complex spike response to air-puff
553 stimulation probably acted as a permissive gate to increase the simple spike response
554 following training, which is in line with current theories on cerebellar plasticity (Coesmans et
555 al., 2004, Ito, 2001, Lev-Ram et al., 2002, Ohtsuki et al., 2009). The PCs with a relatively
556 high complex spike response probability were not prone for increases in simple spike activity
557 following our training protocol. Instead, they may dynamically enhance reflexive whisker
558 protraction through increases in their coherent complex spike firing, likely engaging ensemble
559 encoding (Hoogland et al., 2015, Mukamel et al., 2009, Ozden et al., 2009, Schultz et al.,
560 2009). This enhancement does not require a repetitive training protocol and also occurs during
561 single trial stimulation. Indeed, these complex spike responses, which tended to precede the
562 active whisker movement, could be correlated to the strength of the touch-induced whisker
563 protraction under baseline conditions. This is in line with previous studies showing that

564 complex spikes can facilitate the initiation of movements and define their amplitude
565 (Hoogland et al., 2015, Kitazawa et al., 1998, Welsh et al., 1995). Thus, PCs with strong
566 complex spike responses to whisker stimulation – especially those located in the D2 zone of
567 crus 1 – show poor simple spike enhancement to mediate whisker adaptation, but they might
568 facilitate execution of touch-induced whisker protraction under baseline conditions by
569 relaying coherent patterns of complex spikes onto the cerebellar nuclei neurons.
570
571 *Conclusion*
572 Based on a known form of reflexive whisker movements, we introduced a novel adaptation
573 paradigm and investigated the underlying cerebellar plasticity mechanism and spiking
574 learning rules. A brief period of increased sensory input appeared to be sufficient to induce a
575 lasting impact on touch-induced whisker protraction: the whisker reflex started earlier and had
576 a bigger amplitude. This motor adaptation probably requires induction of parallel fiber LTP in
577 PCs that can be identified by their weak but present complex spike response to sensory
578 stimulation. The resultant increased simple spike firing of these PCs may affect the brainstem
579 loop controlling touch-induced whisker protraction via the reticular formation in the
580 brainstem, in line with optogenetic stimulation experiments. Thus, our study proposes
581 induction of parallel fiber to PC LTP as a cellular mechanism for enhancing PC simple spike
582 responsiveness that facilitates the expression of the entrained whisker protraction.

Acknowledgements

Financial support was provided by the Netherlands Organization for Scientific Research (NWO-ALW; C.I.D.Z.), the Dutch Organization for Medical Sciences (ZonMW; C.I.D.Z.), Life Sciences (C.I.D.Z.), ERC-adv and ERC-POC (C.I.D.Z.) and the China Scholarship Council (No. 2010623033; C.J.). We thank E. Haasdijk, E. Goedknegt, M. Rutteman, and A.C.H.G. IJpelaar for technical assistance and Drs. T.J.H. Ruigrok, S.K.E. Koekkoek, J.J. White and M. Schonewille of the Neuroscience Department at the Erasmus Medical Center for their input and scientific discussions, as well as Dr. D. Rizopoulos of the Biostatistics Department at the Erasmus Medical Center and Dr. D. Vidotto from Tilburg University for statistical consulting regarding the cluster analysis.

Competing financial interests

The authors declare no competing financial interests.

Materials and methods

Key Resource Table

Resource	Designation	Source	Identifiers
Strains	Tg(Pcp2-cre)2MPin;Ppp3r1^{tm1Stl}	(Schonewille et al., 2010)	N/A
	Tg(Pcp2-cre)2MPin;Gria3^{tm2Rsp}	(Gutierrez-Castellanos et al., 2017)	N/A
	C57Bl6J mice	Charles Rivers	IMSR_JAX:000664
	Tg(Pcp2-cre)2Mpin:: Gt(ROSA)26Sor$^{tm27.1(CAG-OP4*H134R/tdTomato)Hze}$	(Witter et al., 2013)	N/A
	Dextran, Biotin, 3000 MW, Lysine Fixable (BDA-3000)	Thermo Fisher Scientific	D7135
	Paraformaldehyde	Merck	1.040005.1000
	Thionine	Sigma	T-3387
	Gelatin	J.T.Baker	2124-01
Software	MATLAB v2012a-v2017a	Mathworks	
	LabVIEW (for video acquisition)	National Instruments	
	BWTT Toolbox (for whisker tracking)	http://bwtt.sourceforge.net	

Animals

In this study, we used two different mutant mouse lines, both on a C57Bl/6J background. Comparisons of electrophysiological parameters were always made between the mutant mice and their respective wild-type (WT) littermates, although for easier visualization the WTs were sometimes grouped as indicated in the figure legends. Both mouse lines had been used before and details on their generation have been published. Briefly, L7-PP2B mice (Tg(Pcp2-cre)2MPin;Ppp3r1^{tm1Stl}) lacked functional PP2B specifically in their Purkinje cells (PCs). They were created by crossing mice in which the gene for the regulatory subunit (CNB1) of PP2B was flanked by loxP sites (Zeng et al., 2001) with transgenic mice expressing Cre-recombinase under control of the L7 (Pcp2) promoter (Barski et al., 2000) as described in Schonewille et al. (2010). L7-Cre$^{+/-}$-cnb1$^{f/f}$ mice ("L7-PP2B mice") were compared with L7-Cre$^{-/-}$-cnb1$^{f/f}$ littermate controls. We used 35 WT mice (17 males and 18 females of 21 ± 9 weeks of age (average ± s.d.)) and 22 L7-PP2B mice (6 males and 16 females of 18 ± 10

weeks of age (average ± s.d.)). L7-GluA3 mice (Tg(Pcp2-cre)2MPin;Gria3^{tm2Rsp}) lacked the AMPA receptor GluA3 subunit specifically in their PCs. They were created by crossing mice in which the *Gria3* gene was flanked by loxP sites (Sanchis-Segura et al., 2006) with transgenic mice expressing Cre-recombinase under control of the L7 (Pcp2) promoter (Barski et al., 2000) as described in Gutierrez-Castellanos et al. (2017). We used L7-Cre$^{+/-}$-Gria3$^{f/f}$ mice ("L7-GluA3 mice") and L7-Cre$^{-/-}$-Gria3$^{f/f}$ as littermate controls. We used 5 WT male mice (25 ± 3 weeks of age (average ± s.d.)) and 9 L7-GluA3 mice (6 males and 3 females of 26 ± 4 weeks of age (average ± s.d.)). Mutants and wild-types were measured in random sequence. For the two-photon Ca^{2+} imaging experiments, we used 6 male C57Bl/6J mice (Charles Rivers, Leiden, the Netherlands) of 4-12 weeks of age. The photostimulation experiments were performed on 7 mice (3 males and 4 females of 25 ± 1 weeks of age (average ± s.d.)) expressing Channelrhodopsin-2 exclusively in their PCs (Tg(Pcp2-cre)2MPin;Gt(ROSA)26Sor$^{tm27.1(CAG-COP4*H134R/tdTomato)Hze}$) as described previously (Witter et al., 2013). All mice were socially housed until surgery and single-housed afterwards. The mice were kept at a 12/12 h light/dark cycle and had not been used for any invasive procedure (except genotyping shortly after birth) before the start of the experiment. All mice used were specific-pathogen free (SPF). All experimental procedures were approved a priori by an independent animal ethical committee (DEC-Consult, Soest, The Netherlands) as required by Dutch law and conform the relevant institutional regulations of the Erasmus MC and Dutch legislation on animal experimentation.

Surgery

All mice that were used for electrophysiology received a magnetic pedestal that was attached to the skull above bregma using Optibond adhesive (Kerr Corporation, Orange, CA) and a craniotomy was made on top of crus 1 and crus 2. The surgical procedures were performed

under isoflurane anesthesia (2-4% V/V in O_2). Post-surgical pain was treated with 5 mg/kg carprofen ("Rimadyl", Pfizer, New York, NY, USA), 1 µg lidocaine (Braun, Meisingen, Germany), 1 µg bupivacaine (Actavis, Parsippany-Troy Hills, NJ, USA) and 50 µg/kg buprenorphine ("Temgesic", Indivior, Richmond, VA, USA). After three days of recovery, mice were habituated to the recording setup during at least 2 daily sessions of approximately 45 min. In the recording setup they were head-fixed using the magnetic pedestal. The mice used for two-photon imaging received a head plate with a sparing on the location of the craniotomy instead of a pedestal. The head plate was attached to the skull with dental cement (Superbond C&B, Sun Medical Co., Moriyama City, Japan). To prevent the growth of scar tissue, which could affect image quality, two-photon recordings were made on the day of the surgery (recording started at least 1 h after the termination of anesthesia).

Whisker stimulation and tracking

Air-puff stimulation to the whisker pad was applied with a frequency of 0.5 Hz s at a distance of approximately 3 mm at an angle of approximately 35° (relative to the body axis). The puffs were delivered using a tube with a diameter of approximately 1 mm with a pressure of ~2 bar and a duration of 30 ms. During the induction period, the stimulation frequency was increased to 4 Hz and 80 puffs were given. In a subset of experiments, a 2 ms air-puff (pre-pulse) was delivered 100 ms prior to the 30 ms puff. Videos of the whiskers were made from above using a bright LED panel as backlight (λ = 640 nm) at a frame rate of 1,000 Hz (480x500 pixels using an A504k camera from Basler Vision Technologies, Ahrensburg, Germany). The whiskers were not trimmed or cut.

663 *Electrophysiology*

664 Electrophysiological recordings were performed in awake L7-PP2B WT mice using either
665 glass pipettes (3-6 MΩ) or quartz-coated platinum/tungsten electrodes (2-5 MΩ, outer
666 diameter = 80 µm, Thomas Recording, Giessen, Germany). The latter electrodes were placed
667 in an 8x4 matrix (Thomas Recording), with an inter-electrode distance of 305 µm. Prior to the
668 recordings, the mice were lightly anesthetized with isoflurane to remove the dura, bring them
669 in the setup and adjust all manipulators. Recordings started at least 60 min after termination of
670 anesthesia and were made in crus 1 and crus 2 ipsilateral to the side of the whisker pad
671 stimulation at a minimal depth of 500 µm. The electrophysiological signal was digitized at 25
672 kHz, using a 1-6,000 Hz band-pass filter, 22x pre-amplified and stored using a RZ2 multi-
673 channel workstation (Tucker-Davis Technologies, Alachua, FL).

674

675 *Neural tracing & electrolytic lesions*

676 For the neural tracing experiments, we used glass electrodes filled with 2 M NaCl for
677 juxtacellular recordings. After a successful recording of a PC, neural tracer was pressure
678 injected (3 x 10 ms with a pressure of 0.7 bar) either from the same pipette re-inserted at the
679 same location or from the second barrel or a double barrel pipette. We used a gold-lectin
680 conjugate has described previously (Ruigrok et al., 1995) (n = 3) or biotinylated dextran
681 amine (BDA) 3000 (10 mg/ml in 0.9% NaCl; ThermoFisher Scientific, Waltham, MA, USA)
682 (n = 7). Five days after the tracer injection, the mice were anesthetized with pentobarbital (80
683 mg/kg intraperitoneal) and fixated by transcardial perfusion with 4% paraformaldehyde. The
684 brains were removed and sliced (40 µm thick). The slices were processed by Nissl staining.
685 Experiments were included in the analysis if the electrophysiology fulfilled the requirements
686 mentioned above with a recording duration of at least 50 s and if the tracer was clearly visible.
687 For BDA 3000 this implied that it was taken up by the PCs at the injection spot and

transported to the axonal boutons a single subgroup in the cerebellar nuclei. BDA 3000 was also found in the inferior olive. For the gold-lectin conjugate the subnucleus of the inferior olive was considered. Based upon the subnuclei of the cerebellar nuclei and/or the inferior olive, the sagittal zone of the recording site was identified according to the scheme published in Apps and Hawkes (2009).

After the recordings made with the quartz/platinum electrodes, electrolytic lesions were applied to selected electrodes in order to retrieve the recording locations. To this end, we applied a DC current of 20 µA for 20 s. This typically resulted in a lesion that could be visualized after Nissl staining of 40 µm thick slices made of perfused brains. We accepted a spot as a true lesion if it was visible in at least 2 consecutive slices at the same location. In total, we could retrieve 16 successful lesions. Recording locations were approximated using pictures of the entry points of the electrodes in combination with the locations of the lesions.

Two-photon Ca^{2+} imaging

After the surgery (see above) with the dura mater intact, the surface of the cerebellar cortex was rinsed with extracellular solution composed of (in mM) 150 NaCl, 2.5 KCl, 2 $CaCl_2$, 1 $MgCl_2$ and 10 HEPES (pH 7.4, adjusted with NaOH). After a 30 minute recovery period from anesthesia animals were head-fixed in the recording setup and received a bolus-loading of the cell-permeant fluorescent Ca^{2+} indicator Cal-520 AM (0.2 mM; AAT Bioquest, Sunnyvale, CA, USA). The dye was first dissolved with 10% w/V Pluronic F-127 in DMSO (Invitrogen) and diluted 20x in the extracellular solution. The dye solution was pressure injected into the molecular layer (50–80 µm below the surface) at 0.35 bar for 5 min. After dye loading, the brain surface was covered with 2% agarose dissolved in saline (0.9% NaCl) in order to reduce motion artefacts and prevent dehydration.

712 Starting at least 30 min after dye injection, *in vivo* two-photon Ca^{2+} imaging was
713 performed of the molecular layer using a setup consisting of a titanium sapphire laser
714 (Chameleon Ultra, Coherent, Santa Clara, CA), a TriM Scope II system (LaVisionBioTec,
715 Bielefeld, Germany) mounted on a BX51 microscope with a 20x 1.0 NA water immersion
716 objective (Olympus, Tokyo, Japan) and GaAsP photomultiplier detectors (Hamamatsu, Iwata
717 City, Japan). A typical recording sampled 40 x 200 µm with a frame rate of approximately 25
718 Hz.
719
720 *Data inclusion*
721 We included all mice measured during this study, with the exception of one mouse where
722 video-analysis revealed that the air-puff was delivered more to the nose than to the whisker
723 pad. Single-unit data was included if the recording was of sufficient quality and reflected the
724 activity of a single PC according to the rules defined below (see section *Electrophysiological*
725 *analysis*).
726
727 *Whisker tracking*
728 Whisker movements were tracked offline as described previously (Rahmati et al., 2014) using
729 a method based on the BIOTACT Whisker Tracking Tool (Perkon et al., 2011). We used the
730 average angle of all trackable large facial whiskers for further quantification of whisker
731 behavior. The impact of 4 Hz air-puff stimulation on air-puff-triggered whisker movement
732 was quantified using a bootstrap method. First, we took the last 100 trials before induction
733 and divided these randomly in two series of 50. We calculated the differences in whisker
734 position between these two series, and repeated this 1000 times. From this distribution we
735 derived the expected variation after whisker pad air-puff stimulation. We took the 99%

736 confidence interval as the threshold to which we compared the difference between 50
737 randomly chosen trials after and 50 randomly chosen trials before induction.
738
739 *Electrophysiological analysis*
740 Spikes were detected offline using SpikeTrain (Neurasmus, Rotterdam, The Netherlands). A
741 recording was considered to originate from a single PC when it contained both complex
742 spikes (identified by the presence of stereotypic spikelets) and simple spikes, when the
743 minimal inter-spike interval of simple spikes was 3 ms and when each complex spike was
744 followed by a pause in simple spike firing of at least 8 ms. The regularity of simple spike
745 firing was expressed as the local variation (CV2) and calculated as $2|ISI_{n+1}-ISI_n|/(ISI_{n+1}+ISI_n)$
746 with ISI = inter-simple spike interval (Shin et al., 2007). Only single-unit recordings of PCs
747 with a minimum recording duration of 200 s were selected for further analysis. However, for
748 the neural tracing experiments (see below), on which no quantitative analysis was performed,
749 we accepted a minimum recording duration of 50 s.
750
751 *Two-photon Ca^{2+} imaging analysis*
752 Image analysis was performed offline using custom made software as described and validated
753 previously (Ozden et al., 2008, Ozden et al., 2012, De Gruijl et al., 2014). In short, we
754 performed independent component analysis to define the areas of individual Purkinje cell
755 dendrites (Figure 3 – figure supplement 2A). The fluorescent values of all pixels in each
756 region of interest were averaged per frame. These averages were plotted over time using a
757 high-pass filter. A 8% rolling baseline was subtracted with a time window of 0.5 ms (Ozden
758 et al., 2012). Ca^{2+} transients were detected using template matching. For the aggregate peri-
759 stimulus time histograms (PSTHs), we calculated per individual frame the number of complex
760 spikes detected and made a PSTH color coding the number of simultaneously detected

761 complex spikes. Based on the total number of complex spikes and dendrites per recording, we
762 calculated the expected number of simultaneous complex spikes per individual frame based
763 upon a Poisson distribution. The actual number of simultaneous complex spikes was
764 compared to this calculated distribution and a *p* value was derived for each number based
765 upon the Poisson distribution.
766
767 *Characterization of sensory responses*
768 For each PC recording, we constructed PSTHs of complex spikes and simple spikes
769 separately using a bin size of 10 ms for display purposes. For further quantitative analyses of
770 the PSTHs, we used a bin size of 1 ms and convolved them with a 21 ms wide Gaussian
771 kernel. Complex spike responses were characterized by their peak amplitude, defined as the
772 maximum of the convolved PSTH and expressed in percentage of trials in which a complex
773 spike occurred within a 1 ms bin. Latencies were taken as the time between stimulus onset
774 and the time of the response peak, as determined from the convolved PSTH. For some
775 analyses, we discriminated between the sensory response period (0-60 ms after stimulus
776 onset) and inter-trial interval (500 to 200 ms before stimulus onset). We considered a PC
777 responsive for sensory stimulation if the peak or trough in the PSTH in the 60 ms after the
778 stimulus onset exceeded the threshold of 3 s.d. above or below the average of the pre-stimulus
779 interval (1 ms bins convolved with a 21 ms Gaussian kernel, pre-stimulus interval 200 ms
780 before stimulus onset). Long-term stability of electrophysiological recordings was verified by
781 heat maps of time-shifted PSTHs. The time-shifted PSTH was processed by calculating the
782 simple spike PSTH for 20 air-puffs per row, which were shifted by 5 air-puffs between
783 neighboring rows. The simple spike rates per row are calculated at 1 ms resolution and
784 convolved with a 21 ms Gaussian kernel and color-coded relative to baseline firing rate (-
785 1000 to -200 ms relative to air-puff time).

Cluster analysis

A principal component analysis showed that the heterogeneity among the sensory complex spike responses was driven almost exclusively by one parameter, the maximum amplitude peak of the convolved complex spike PSTH. We performed a univariate Gaussian mixture model using only that variable. The Bayesian information criterion (BIC) indicated that the model with two components with unequal variances yielded the best approximation of the data. Then we applied the function Mclust(data) in R (R Foundation, Vienna, Austria) which use the expectation-maximization algorithm in order to assert the main parameters of the resulting models (probability, mean and variance of each population).

Spike-whisker movement correlation matrix

Trial-by-trial correlation between instantaneous simple spike firing rate and whisker position was performed as described before (Ten Brinke et al., 2015). In short: spike density functions were computed for all trials by convolving spike occurrences across 1 ms bins with an 8 ms Gaussian kernel. Both spike and whisker data were aligned to the 200 ms baseline. For cell groups, data was standardized for each cell for each correlation, and then pooled. The spike-whisker Pearson correlation coefficient R was calculated in bin of 10 ms, resulting in a 40x40 R-value matrix showing correlations for -100 to 300 ms around the air-puff presentation.

Statistical analysis

Group sizes of the blindly acquired data sets were not defined a priori as the effect size and variation were not known beforehand. A post hoc power calculation based upon the results of the potentiation of the PC responses to whisker pad stimulation of the "weak complex spike responders" indicated a minimum group size of 12 PCs (α = 5%, β = 20%, Δ = 9.65%, s.d. = 10.59%, paired *t* test). This number was obtained for the "weak complex spike responders" in

WT (n = 35), L7-PP2B (n = 21) and L7-GluA3 PCs (n = 13), as well as for the relatively rare "strong complex spike responders" in WT mice (n = 20). This was further substantiated by other independent analyses, including ANOVA and linear regression, as described in the Results section. Variations in success rate, especially considering recordings of longer duration in combination with video tracking, explain why some groups are larger than others. Data was excluded only in case of a signal to noise ratio that was insufficient to warrant reliable analysis. For data visualization and statistical analysis, we counted the number of PCs as the number of replicates for the spike-based analyses and the number of mice for the behavior-based analyses. We tested whether the observed increase in coherence after sensory stimulation (Figure 3 – figure supplement 2D-G) was more than expected from the increased firing rate induced by the stimulation. The expected coherence based on the firing rate was calculated from 1000 bootstrapped traces from the inhomogeneous Poisson spike trains made for each neuron. The resultant distribution was compared to the measured distribution using a two-sample Kolmogorov-Smirnov test. Stacked line plots were generated by cumulating the values of all subjects per time point. Thus, the first line (darkest color) represents the first subject, the second line the sum of the first two, the third line the first three, etcetera. The data are divided by the number of subjects, so that the last line (brightest color) represents, next to the increase from the one but last value, also the population average. Sample size and measures for mean and variation are specified throughout the text and figure legends. For normally distributed data (as evaluated using the Kolmogorov-Smirnov test) parametric tests were used. Comparisons were always made with 2-sided tests when applicable. Unpaired t test were always made with Welch correction for possible differences in s.d.

833 *Data and software availability*

834 All relevant data is available from the authors. Custom written Matlab code to complement
835 the whisker tracking analysis by the BIOTACT Whisker Tracking Tool was used as described
836 previously (Rahmati et al., 2014) and can be obtained from the authors.

837 **References**

838

839 Ahl, A. S. 1986. The role of vibrissae in behavior: a status review. *Vet Res Commun,* 10**,** 245-
840 68, 10.1007/BF02213989.
841 Albus, J. S. 1971. Theory of cerebellar function. *Math Biosci,* 10**,** 25-61, 10.1016/0025-
842 5564(71)90051-4.
843 Anjum, F. & Brecht, M. 2012. Tactile experience shapes prey-capture behavior in Etruscan
844 shrews. *Front Behav Neurosci,* 6**,** 28, 10.3389/fnbeh.2012.00028.
845 Apps, R. & Hawkes, R. 2009. Cerebellar cortical organization: a one-map hypothesis. *Nat Rev*
846 *Neurosci,* 10**,** 670-81, 10.1038/nrn2698.
847 Arkley, K., Tiktak, G. P., Breakell, V., Prescott, T. J. & Grant, R. A. 2017. Whisker touch
848 guides canopy exploration in a nocturnal, arboreal rodent, the Hazel dormouse
849 (*Muscardinus avellanarius*). *J Comp Physiol A Neuroethol Sens Neural Behav*
850 *Physiol,* 203**,** 133-142, 10.1007/s00359-017-1146-z.
851 Badura, A., Schonewille, M., Voges, K., Galliano, E., Renier, N., Gao, Z., Witter, L.,
852 Hoebeek, F. E., Chedotal, A. & De Zeeuw, C. I. 2013. Climbing fiber input shapes
853 reciprocity of Purkinje cell firing. *Neuron,* 78**,** 700-13, 10.1016/j.neuron.2013.03.018.
854 Barski, J. J., Dethleffsen, K. & Meyer, M. 2000. Cre recombinase expression in cerebellar
855 Purkinje cells. *Genesis,* 28**,** 93-8, 10.1002/1526-968X(200011/12)28:3/4<93::AID-
856 GENE10>3.0.CO;2-W.
857 Bellavance, M. A., Takatoh, J., Lu, J., Demers, M., Kleinfeld, D., Wang, F. & Deschênes, M.
858 2017. Parallel inhibitory and excitatory trigemino-facial feedback circuitry for
859 reflexive vibrissa movement. *Neuron,* 95**,** 673-82, 10.1016/j.neuron.2017.06.045.

860 Berg, R. W. & Kleinfeld, D. 2003. Rhythmic whisking by rat: retraction as well as protraction
861 of the vibrissae is under active muscular control. *J Neurophysiol,* 89**,** 104-17,
862 10.1152/jn.00600.2002.
863 Boele, H. J., Peter, S., Ten Brinke, M. M., Verdonschot, L., IJpelaar, A. C. H. G., Rizopoulos,
864 D., Gao, Z., Koekkoek, S. K. E. & De Zeeuw, C. I. in press. Impact of parallel fiber to
865 Purkinje cell long-term depression is unmasked in absence of inhibitory input. *Sci*
866 *Adv*,
867 Bosman, L. W. J., Houweling, A. R., Owens, C. B., Tanke, N., Shevchouk, O. T., Rahmati,
868 N., Teunissen, W. H. T., Ju, C., Gong, W., Koekkoek, S. K. E. & De Zeeuw, C. I.
869 2011. Anatomical pathways involved in generating and sensing rhythmic whisker
870 movements. *Front Integr Neurosci,* 5**,** 53, 10.3389/fnint.2011.00053.
871 Bosman, L. W. J., Koekkoek, S. K. E., Shapiro, J., Rijken, B. F. M., Zandstra, F., van der
872 Ende, B., Owens, C. B., Potters, J. W., de Gruijl, J. R., Ruigrok, T. J. H. & De Zeeuw,
873 C. I. 2010. Encoding of whisker input by cerebellar Purkinje cells. *J Physiol,* 588**,**
874 3757-83, doi:10.1113/jphysiol.2010.195180.
875 Brecht, M. 2007. Barrel cortex and whisker-mediated behaviors. *Curr Opin Neurobiol,* 17**,**
876 408-16, 10.1016/j.conb.2007.07.008.
877 Brown, I. E. & Bower, J. M. 2001. Congruence of mossy fiber and climbing fiber tactile
878 projections in the lateral hemispheres of the rat cerebellum. *J Comp Neurol,* 429**,** 59-
879 70, 10.1002/1096-9861(20000101)429:1<59::AID-CNE5>3.0.CO;2-3 [pii].
880 Brown, S. T. & Raman, I. M. 2018. Sensorimotor integration and amplification of reflexive
881 whisking by well-timed spiking in the cerebellar corticonuclear circuit. *Neuron,*
882 10.1016/j.neuron.2018.06.028.
883 Chaumont, J., Guyon, N., Valera, A. M., Dugué, G. P., Popa, D., Marcaggi, P., Gautheron, V.,
884 Reibel-Foisset, S., Dieudonné, S., Stephan, A., Barrot, M., Cassel, J. C., Dupont, J. L.,

885 Doussau, F., Poulain, B., Selimi, F., Léna, C. & Isope, P. 2013. Clusters of cerebellar
886 Purkinje cells control their afferent climbing fiber discharge. *Proc Natl Acad Sci U S*
887 *A*, 110**,** 16223-8, 10.1073/pnas.1302310110.
888 Chen, S., Augustine, G. J. & Chadderton, P. 2016. The cerebellum linearly encodes whisker
889 position during voluntary movement. *Elife*, 5**,** e10509, 10.7554/eLife.10509.
890 Chu, C. P., Bing, Y. H. & Qiu, D. L. 2011. Sensory stimulus evokes inhibition rather than
891 excitation in cerebellar Purkinje cells *in vivo* in mice. *Neurosci Lett,* 487**,** 182-6,
892 10.1016/j.neulet.2010.10.018.
893 Coesmans, M., Weber, J. T., De Zeeuw, C. I. & Hansel, C. 2004. Bidirectional parallel fiber
894 plasticity in the cerebellum under climbing fiber control. *Neuron,* 44**,** 691-700,
895 10.1016/j.neuron.2004.10.031.
896 D'Angelo, E., Mapelli, L., Casellato, C., Garrido, J. A., Luque, N., Monaco, J., Prestori, F.,
897 Pedrocchi, A. & Ros, E. 2016. Distributed circuit plasticity: new clues for the
898 cerebellar mechanisms of learning. *Cerebellum,* 15**,** 139-51, 10.1007/s12311-015-
899 0711-7.
900 D'Angelo, E., Nieus, T., Maffei, A., Armano, S., Rossi, P., Taglietti, V., Fontana, A. & Naldi,
901 G. 2001. Theta-frequency bursting and resonance in cerebellar granule cells:
902 experimental evidence and modeling of a slow k+-dependent mechanism. *J Neurosci,*
903 21**,** 759-70, 10.1523/JNEUROSCI.21-03-00759.2001.
904 De Gruijl, J. R., Hoogland, T. M. & De Zeeuw, C. I. 2014. Behavioral correlates of complex
905 spike synchrony in cerebellar microzones. *J Neurosci,* 34**,** 8937-44,
906 10.1523/JNEUROSCI.5064-13.2014.
907 De Zeeuw, C. I., Hoebeek, F. E., Bosman, L. W. J., Schonewille, M., Witter, L. & Koekkoek,
908 S. K. 2011. Spatiotemporal firing patterns in the cerebellum. *Nat Rev Neurosci,* 12**,**
909 327-44, doi:10.1038/nrn3011.

De Zeeuw, C. I., Lang, E. J., Sugihara, I., Ruigrok, T. J., Eisenman, L. M., Mugnaini, E. & Llinás, R. 1996. Morphological correlates of bilateral synchrony in the rat cerebellar cortex. *J Neurosci,* 16**,** 3412-26, 10.1523/JNEUROSCI.16-10-03412.1996.

De Zeeuw, C. I. & Ten Brinke, M. M. 2015. Motor learning and the cerebellum. *Cold Spring Harb Perspect Biol,* 7**,** a021683, 10.1101/cshperspect.a021683.

De Zeeuw, C. I., Wylie, D. R., Stahl, J. S. & Simpson, J. I. 1995. Phase relations of Purkinje cells in the rabbit flocculus during compensatory eye movements. *J Neurophysiol,* 74**,** 2051-64, 10.1152/jn.1995.74.5.2051.

Dehnhardt, G., Mauck, B., Hanke, W. & Bleckmann, H. 2001. Hydrodynamic trail-following in harbor seals (*Phoca vitulina*). *Science,* 293**,** 102-4, 10.1126/science.1060514.

Dere, E., Huston, J. P. & De Souza Silva, M. A. 2007. The pharmacology, neuroanatomy and neurogenetics of one-trial object recognition in rodents. *Neurosci Biobehav Rev,* 31**,** 673-704, 10.1016/j.neubiorev.2007.01.005.

Deschênes, M., Takatoh, J., Kurnikova, A., Moore, J. D., Demers, M., Elbaz, M., Furuta, T., Wang, F. & Kleinfeld, D. 2016. Inhibition, not excitation, drives rhythmic whisking. *Neuron,* 90**,** 374-87, 10.1016/j.neuron.2016.03.007.

Ferezou, I., Haiss, F., Gentet, L. J., Aronoff, R., Weber, B. & Petersen, C. C. H. 2007. Spatiotemporal dynamics of cortical sensorimotor integration in behaving mice. *Neuron,* 56**,** 907-23., 10.1016/j.neuron.2007.10.007.

Gao, Z., Van Beugen, B. J. & De Zeeuw, C. I. 2012. Distributed synergistic plasticity and cerebellar learning. *Nat Rev Neurosci,* 13**,** 619-35, 10.1038/nrn3312.

Gogan, P. 1970. The startle and orienting reactions in man. A study of their characteristics and habituation. *Brain Res,* 18**,** 117-35, 10.1016/0006-8993(70)90460-9.

Gutierrez-Castellanos, N., Da Silva-Matos, C. M., Zhou, K., Canto, C. B., Renner, M. C., Koene, L. M. C., Ozyildirim, O., Sprengel, R., Kessels, H. W. & De Zeeuw, C. I.

2017. Motor learning requires Purkinje cell synaptic potentiation through activation of AMPA-receptor subunit GluA3. *Neuron,* 93**,** 409-424, 10.1016/j.neuron.2016.11.046.

Haidarliu, S., Kleinfeld, D., Deschênes, M. & Ahissar, E. 2015. The musculature that drives active touch by vibrissae and nose in mice. *Anat Rec (Hoboken),* 298**,** 1347-58, 10.1002/ar.23102.

Halverson, H. E., Khilkevich, A. & Mauk, M. D. 2015. Relating cerebellar Purkinje cell activity to the timing and amplitude of conditioned eyelid responses. *J Neurosci,* 35**,** 7813-32, 10.1523/JNEUROSCI.3663-14.2015.

Hansel, C., Linden, D. J. & D'Angelo, E. 2001. Beyond parallel fiber LTD: the diversity of synaptic and non-synaptic plasticity in the cerebellum. *Nat Neurosci,* 4**,** 467-75, 10.1038/87419.

Heiney, S. A., Wohl, M. P., Chettih, S. N., Ruffolo, L. I. & Medina, J. F. 2014. Cerebellar-dependent expression of motor learning during eyeblink conditioning in head-fixed mice. *J Neurosci,* 34**,** 14845-53, 10.1523/JNEUROSCI.2820-14.2014.

Herfst, L. J. & Brecht, M. 2008. Whisker movements evoked by stimulation of single motor neurons in the facial nucleus of the rat. *J Neurophysiol,* 99**,** 2821-32, 01014.2007 [pii]

10.1152/jn.01014.2007.

Herzfeld, D. J., Kojima, Y., Soetedjo, R. & Shadmehr, R. 2015. Encoding of action by the Purkinje cells of the cerebellum. *Nature,* 526**,** 439-42, 10.1038/nature15693.

Herzfeld, D. J., Kojima, Y., Soetedjo, R. & Shadmehr, R. 2018. Encoding of error and learning to correct that error by the Purkinje cells of the cerebellum. *Nat Neurosci,* 21**,** 736-743, 10.1038/s41593-018-0136-y.

Hoogland, T. M., De Gruijl, J. R., Witter, L., Canto, C. B. & De Zeeuw, C. I. 2015. Role of synchronous activation of cerebellar Purkinje cell ensembles in multi-joint movement control. *Curr Biol,* 25**,** 1157-65, 10.1016/j.cub.2015.03.009.

960 Ito, M. 2001. Cerebellar long-term depression: characterization, signal transduction, and
961 functional roles. *Physiol Rev,* 81**,** 1143-95., 10.1152/physrev.2001.81.3.1143.
962 Ito, M. 2003. Long-term depression. *Annu Rev Neurosci,* 12**,** 85-102,
963 10.1146/annurev.ne.12.030189.000505.
964 Jirenhed, D. A., Bengtsson, F. & Hesslow, G. 2007. Acquisition, extinction, and reacquisition
965 of a cerebellar cortical memory trace. *J Neurosci,* 27**,** 2493-502,
966 10.1523/JNEUROSCI.4202-06.2007.
967 Ju, C., Bosman, L. W. J., Hoogland, T. M., Velauthapillai, A., Murugesan, P., Warnaar, P.,
968 Negrello, M. & De Zeeuw, C. I. 2018. Neurons of the inferior olive respond to broad
969 classes of sensory input while subject to homeostatic control. *bioRxiv***,** 379149,
970 10.1101/379149.
971 Kitazawa, S., Kimura, T. & Yin, P. B. 1998. Cerebellar complex spikes encode both
972 destinations and errors in arm movements. *Nature,* 392**,** 494-7, 10.1038/33141.
973 Kleinfeld, D., Berg, R. W. & O'Connor, S. M. 1999. Anatomical loops and their electrical
974 dynamics in relation to whisking by rat. *Somatosens Mot Res,* 16**,** 69-88,
975 Koekkoek, S. K. E., Hulscher, H. C., Dortland, B. R., Hensbroek, R. A., Elgersma, Y.,
976 Ruigrok, T. J. H. & De Zeeuw, C. I. 2003. Cerebellar LTD and learning-dependent
977 timing of conditioned eyelid responses. *Science,* 301**,** 1736-9,
978 10.1126/science.1088383.
979 Konnerth, A., Dreessen, J. & Augustine, G. J. 1992. Brief dendritic calcium signals initiate
980 long-lasting synaptic depression in cerebellar Purkinje cells. *Proc Natl Acad Sci U S*
981 *A,* 89**,** 7051-5., 10.1073/pnas.89.15.7051.
982 Kubo, R., Aiba, A. & Hashimoto, K. 2018. The anatomical pathway from the
983 mesodiencephalic junction to the inferior olive relays perioral sensory signals to the
984 cerebellum in the mouse. *J Physiol,* 10.1113/JP275836.

985 Lev-Ram, V., Mehta, S. B., Kleinfeld, D. & Tsien, R. Y. 2003. Reversing cerebellar long-
986 term depression. *Proc Natl Acad Sci U S A,* 100**,** 15989-93,
987 10.1073/pnas.2636935100.
988 Lev-Ram, V., Wong, S. T., Storm, D. R. & Tsien, R. Y. 2002. A new form of cerebellar long-
989 term potentiation is postsynaptic and depends on nitric oxide but not cAMP. *Proc Natl*
990 *Acad Sci U S A,* 99**,** 8389-93., 10.1073/pnas.122206399.
991 Lisberger, S. G. 1998. Physiologic basis for motor learning in the vestibulo-ocular reflex.
992 *Otolaryngol Head Neck Surg,* 119**,** 43-8, 10.1016/S0194-5998(98)70172-X.
993 Lisberger, S. G. & Miles, F. A. 1980. Role of primate medial vestibular nucleus in long-term
994 adaptive plasticity of vestibuloocular reflex. *J Neurophysiol,* 43**,** 1725-45,
995 10.1152/jn.1980.43.6.1725.
996 Loewenstein, Y., Mahon, S., Chadderton, P., Kitamura, K., Sompolinsky, H., Yarom, Y. &
997 Häusser, M. 2005. Bistability of cerebellar Purkinje cells modulated by sensory
998 stimulation. *Nat Neurosci,* 8**,** 202-11, 10.1038/nn1393.
999 Ly, R., Bouvier, G., Schonewille, M., Arabo, A., Rondi-Reig, L., Léna, C., Casado, M., De
1000 Zeeuw, C. I. & Feltz, A. 2013. T-type channel blockade impairs long-term
1001 potentiation at the parallel fiber-Purkinje cell synapse and cerebellar learning. *Proc*
1002 *Natl Acad Sci U S A,* 110**,** 20302-7, 10.1073/pnas.1311686110.
1003 McElvain, L. E., Bagnall, M. W., Sakatos, A. & du Lac, S. 2010. Bidirectional plasticity
1004 gated by hyperpolarization controls the gain of postsynaptic firing responses at central
1005 vestibular nerve synapses. *Neuron,* 68**,** 763-75, 10.1016/j.neuron.2010.09.025.
1006 McElvain, L. E., Friedman, B., Karten, H. J., Svoboda, K., Wang, F., Deschênes, M. &
1007 Kleinfeld, D. 2018. Circuits in the rodent brainstem that control whisking in concert
1008 with other orofacial motor actions. *Neuroscience,* 368**,** 152-170,
1009 10.1016/j.neuroscience.2017.08.034.

1010 Medina, J. F. & Lisberger, S. G. 2008. Links from complex spikes to local plasticity and
1011 motor learning in the cerebellum of awake-behaving monkeys. *Nat Neurosci,* 11**,**
1012 1185-92, 10.1038/nn.2197.
1013 Moreno-Paublete, R., Canlon, B. & Cederroth, C. R. 2017. Differential neural responses
1014 underlying the inhibition of the startle response by pre-pulses or gaps in mice. *Front*
1015 *Cell Neurosci,* 11**,** 19, 10.3389/fncel.2017.00019.
1016 Mukamel, E. A., Nimmerjahn, A. & Schnitzer, M. J. 2009. Automated analysis of cellular
1017 signals from large-scale calcium imaging data. *Neuron,* 63**,** 747-60,
1018 10.1016/j.neuron.2009.08.009.
1019 Narain, D., Remington, E. D., De Zeeuw, C. I. & Jazayeri, M. 2018. A cerebellar mechanism
1020 for learning prior distributions of time intervals. *Nat Commun,* 9**,** 469,
1021 10.1038/s41467-017-02516-x.
1022 Nguyen, Q. T. & Kleinfeld, D. 2005. Positive feedback in a brainstem tactile sensorimotor
1023 loop. *Neuron,* 45**,** 447-57, 10.1016/j.neuron.2004.12.042.
1024 Ohtsuki, G., Piochon, C. & Hansel, C. 2009. Climbing fiber signaling and cerebellar gain
1025 control. *Front Cell Neurosci,* 3**,** 4, 10.3389/neuro.03.004.2009.
1026 Ozden, I., Dombeck, D. A., Hoogland, T. M., Tank, D. W. & Wang, S. S. 2012. Widespread
1027 state-dependent shifts in cerebellar activity in locomoting mice. *PLoS One,* 7**,** e42650,
1028 10.1371/journal.pone.0042650.
1029 Ozden, I., Lee, H. M., Sullivan, M. R. & Wang, S. S. H. 2008. Identification and clustering of
1030 event patterns from in vivo multiphoton optical recordings of neuronal ensembles. *J*
1031 *Neurophysiol,* 100**,** 495-503, 01310.2007 [pii] 10.1152/jn.01310.2007.
1032 Ozden, I., Sullivan, M. R., Lee, H. M. & Wang, S. S. H. 2009. Reliable coding emerges from
1033 coactivation of climbing fibers in microbands of cerebellar Purkinje neurons. *J*
1034 *Neurosci,* 29**,** 10463-73, 10.1523/JNEUROSCI.0967-09.2009.

1035 Perkon, I., Kosir, A., Itskov, P. M., Tasic, J. & Diamond, M. E. 2011. Unsupervised
1036 quantification of whisking and head movement in freely moving rodents. *J*
1037 *Neurophysiol*, 105**,** 1950-62, 10.1152/jn.00764.2010.
1038 Peter, S., Ten Brinke, M. M., Stedehouder, J., Reinelt, C. M., Wu, B., Zhou, H., Zhou, K.,
1039 Boele, H. J., Kushner, S. A., Lee, M. G., Schmeisser, M. J., Boeckers, T. M.,
1040 Schonewille, M., Hoebeek, F. E. & De Zeeuw, C. I. 2016. Dysfunctional cerebellar
1041 Purkinje cells contribute to autism-like behaviour in *Shank2*-deficient mice. *Nat*
1042 *Commun*, 7**,** 12627, 10.1038/ncomms12627.
1043 Prescott, T. J., Diamond, M. E. & Wing, A. M. 2011. Active touch sensing. *Philos Trans R*
1044 *Soc Lond B Biol Sci*, 366**,** 2989-95, 10.1098/rstb.2011.0167.
1045 Proville, R. D., Spolidoro, M., Guyon, N., Dugué, G. P., Selimi, F., Isope, P., Popa, D. &
1046 Léna, C. 2014. Cerebellum involvement in cortical sensorimotor circuits for the
1047 control of voluntary movements. *Nat Neurosci*, 17**,** 1233-9, 10.1038/nn.3773.
1048 Rahmati, N., Owens, C. B., Bosman, L. W. J., Spanke, J. K., Lindeman, S., Gong, W.,
1049 Potters, J. W., Romano, V., Voges, K., Moscato, L., Koekkoek, S. K. E., Negrello, M.
1050 & De Zeeuw, C. I. 2014. Cerebellar potentiation and learning a whisker-based object
1051 localization task with a time response window. *J Neurosci*, 34**,** 1949-62,
1052 10.1523/JNEUROSCI.2966-13.2014.
1053 Ramakrishnan, K. B., Voges, K., De Propris, L., De Zeeuw, C. I. & D'Angelo, E. 2016.
1054 Tactile stimulation evokes long-lasting potentiation of Purkinje cell discharge *in vivo*.
1055 *Front Cell Neurosci*, 10**,** 36, 10.3389/fncel.2016.00036.
1056 Ruigrok, T. J. H., Teune, T. M., van der Burg, J. & Sabel-Goedknegt, H. 1995. A retrograde
1057 double-labeling technique for light microscopy. A combination of axonal transport of
1058 cholera toxin B-subunit and a gold-lectin conjugate. *J Neurosci Methods*, 61**,** 127-38,
1059 10.1016/0165-0270(94)00034-E.

Sanchis-Segura, C., Borchardt, T., Vengeliene, V., Zghoul, T., Bachteler, D., Gass, P., Sprengel, R. & Spanagel, R. 2006. Involvement of the AMPA receptor GluR-C subunit in alcohol-seeking behavior and relapse. *J Neurosci,* 26**,** 1231-8, 10.1523/JNEUROSCI.4237-05.2006.

Schonewille, M., Belmeguenai, A., Koekkoek, S. K., Houtman, S. H., Boele, H. J., van Beugen, B. J., Gao, Z., Badura, A., Ohtsuki, G., Amerika, W. E., Hosy, E., Hoebeek, F. E., Elgersma, Y., Hansel, C. & De Zeeuw, C. I. 2010. Purkinje cell-specific knockout of the protein phosphatase PP2B impairs potentiation and cerebellar motor learning. *Neuron,* 67**,** 618-28, 10.1016/j.neuron.2010.07.009.

Schonewille, M., Gao, Z., Boele, H. J., Vinueza-Veloz, M. F., Amerika, W. E., Simek, A. A. M., De Jeu, M. T., Steinberg, J. P., Takamiya, K., Hoebeek, F. E., Linden, D. J., Huganir, R. L. & De Zeeuw, C. I. 2011. Reevaluating the role of LTD in cerebellar motor learning. *Neuron,* 70**,** 43-50, 10.1016/j.neuron.2011.02.044 [doi].

Schultz, S. R., Kitamura, K., Post-Uiterweer, A., Krupic, J. & Häusser, M. 2009. Spatial pattern coding of sensory information by climbing fiber-evoked calcium signals in networks of neighboring cerebellar Purkinje cells. *J Neurosci,* 29**,** 8005-15, 10.1523/jneurosci.4919-08.2009.

Shin, S. L., Hoebeek, F. E., Schonewille, M., De Zeeuw, C. I., Aertsen, A. & De Schutter, E. 2007. Regular patterns in cerebellar Purkinje cell simple spike trains. *PLoS One,* 2**,** e485, 10.1371/journal.pone.0000485.

Simony, E., Bagdasarian, K., Herfst, L., Brecht, M., Ahissar, E. & Golomb, D. 2010. Temporal and spatial characteristics of vibrissa responses to motor commands. *J Neurosci,* 30**,** 8935-52, 10.1523/JNEUROSCI.0172-10.2010.

1083 Staudacher, E. M., Gebhardt, M. & Dürr, V. 2005. Antennal movements and
1084 mechanoreception: Neurobiology of active tactile sensors. *Adv Insect Physiol*, 32**,** 49-
1085 205, 10.1016/S0065-2806(05)32002-9.
1086 Suvrathan, A., Payne, H. L. & Raymond, J. L. 2016. Timing Rules for Synaptic Plasticity
1087 Matched to Behavioral Function. *Neuron*, 92**,** 959-967, 10.1016/j.neuron.2016.10.022.
1088 Swerdlow, N. R., Caine, S. B., Braff, D. L. & Geyer, M. A. 1992. The neural substrates of
1089 sensorimotor gating of the startle reflex: a review of recent findings and their
1090 implications. *J Psychopharmacol*, 6**,** 176-90, 10.1177/026988119200600210.
1091 Ten Brinke, M. M., Boele, H. J., Spanke, J. K., Potters, J. W., Kornysheva, K., Wulff, P.,
1092 IJpelaar, A. C. H. G., Koekkoek, S. K. E. & De Zeeuw, C. I. 2015. Evolving models of
1093 Pavlovian conditioning: cerebellar cortical dynamics in awake behaving mice. *Cell*
1094 *Rep*, 13**,** 1977-88, 10.1016/j.celrep.2015.10.057.
1095 Teune, T. M., van der Burg, J., van der Moer, J., Voogd, J. & Ruigrok, T. J. 2000.
1096 Topography of cerebellar nuclear projections to the brain stem in the rat. *Prog Brain*
1097 *Res*, 124**,** 141-72, 10.1016/S0079-6123(00)24014-4.
1098 Thier, P., Dicke, P. W., Haas, R., Thielert, C. D. & Catz, N. 2002. The role of the oculomotor
1099 vermis in the control of saccadic eye movements. *Ann N Y Acad Sci*, 978**,** 50-62,
1100 10.1111/j.1749-6632.2002.tb07555.x.
1101 Tsutsumi, S., Yamazaki, M., Miyazaki, T., Watanabe, M., Sakimura, K., Kano, M. &
1102 Kitamura, K. 2015. Structure-function relationships between aldolase C/zebrin II
1103 expression and complex spike synchrony in the cerebellum. *J Neurosci*, 35**,** 843-52,
1104 10.1523/JNEUROSCI.2170-14.2015.
1105 van Beugen, B. J., Gao, Z., Boele, H. J., Hoebeek, F. & De Zeeuw, C. I. 2013. High frequency
1106 burst firing of granule cells ensures transmission at the parallel fiber to purkinje cell

synapse at the cost of temporal coding. *Front Neural Circuits,* 7**,** 95, 10.3389/fncir.2013.00095.

Vincent, S. B. 1913. The tactile hair of the white rat. *J Comp Neurol,* 23**,** 1-36, 10.1002/cne.900230101.

Voges, K., Wu, B., Post, L., Schonewille, M. & De Zeeuw, C. I. 2017. Mechanisms underlying vestibulo-cerebellar motor learning in mice depend on movement direction. *J Physiol,* 595**,** 5301-5326, 10.1113/JP274346.

Voigts, J., Herman, D. H. & Celikel, T. 2015. Tactile object localization by anticipatory whisker motion. *J Neurophysiol,* 113**,** 620-32, 10.1152/jn.00241.2014.

Voogd, J. & Glickstein, M. 1998. The anatomy of the cerebellum. *Trends Neurosci,* 21**,** 370-5, 10.1016/S0166-2236(98)01318-6.

Welker, W. I. 1964. Analysis of sniffing of the albino rat. *Behaviour,* 22**,** 223-244, 10.1163/156853964X00030.

Welsh, J. P., Lang, E. J., Suglhara, I. & Llinas, R. 1995. Dynamic organization of motor control within the olivocerebellar system. *Nature,* 374**,** 453-7, 10.1038/374453a0.

Witter, L., Canto, C. B., Hoogland, T. M., de Gruijl, J. R. & De Zeeuw, C. I. 2013. Strength and timing of motor responses mediated by rebound firing in the cerebellar nuclei after Purkinje cell activation. *Front Neural Circuits,* 7**,** 133, 10.3389/fncir.2013.00133.

Woolsey, T. A., Welker, C. & Schwartz, R. H. 1975. Comparative anatomical studies of the SmI face cortex with special reference to the occurrence of "barrels" in layer IV. *J Comp Neurol,* 164**,** 79-94, 10.1002/cne.901640107.

Yang, Y. & Lisberger, S. G. 2014. Purkinje-cell plasticity and cerebellar motor learning are graded by complex-spike duration. *Nature,* 510**,** 529-32, 10.1038/nature13282.

1130 Yang, Y. & Lisberger, S. G. 2017. Modulation of complex-spike duration and probability
1131 during cerebellar motor learning in visually guided smooth-pursuit eye movements of
1132 monkeys. *eNeuro,* 4, 10.1523/ENEURO.0115-17.2017.
1133 Zeng, H., Chattarji, S., Barbarosie, M., Rondi-Reig, L., Philpot, B. D., Miyakawa, T., Bear,
1134 M. F. & Tonegawa, S. 2001. Forebrain-specific calcineurin knockout selectively
1135 impairs bidirectional synaptic plasticity and working/episodic-like memory. *Cell,* 107**,**
1136 617-29, 10.1016/S0092-8674(01)00585-2.
1137 Zerari-Mailly, F., Pinganaud, G., Dauvergne, C., Buisseret, P. & Buisseret-Delmas, C. 2001.
1138 Trigemino-reticulo-facial and trigemino-reticulo-hypoglossal pathways in the rat. *J*
1139 *Comp Neurol,* 429**,** 80-93,
1140 Zhang, W. & Linden, D. J. 2006. Long-term depression at the mossy fiber-deep cerebellar
1141 nucleus synapse. *J Neurosci,* 26**,** 6935-44, 10.1523/JNEUROSCI.0784-06.2006.
1142 Zhou, H., Lin, Z., Voges, K., Ju, C., Gao, Z., Bosman, L. W. J., Ruigrok, T. J. H., Hoebeek, F.
1143 E., De Zeeuw, C. I. & Schonewille, M. 2014. Cerebellar modules operate at different
1144 frequencies. *eLIFE,* 3**,** e02536, 10.7554/eLife.02536.

1145

Figure legends

Figure 1 | Touch-induced whisker protraction

A brief (30 ms) air-puff to the whisker pad induces a reflexive protraction of all large mystacial whiskers. Our experiments were performed in awake, head-restrained mice that had all whiskers intact. **A.** Photograph showing a part of the mouse head with the large facial whiskers and the location and direction of the air-puffer (top). **B.** The large facial whiskers were recognized in high-speed videos (1 kHz full-frame rate) by a tracking algorithm and individual whiskers are color-coded. **C.** Air-puff stimulation triggered stereotypic whisker movements consisting of an initial passive backwards movement followed by active protraction. Deflection angles of individually tracked whiskers are denoted in distinct colors (same color scheme as in **B**). **D.** The mean whisker angle during 0.5 Hz air-puff stimulation of the whisker pad from a representative mouse. During approximately half the trials, the active protraction was only a single sweep; in the other traces multiple sweeps were observed. Prolonged periods of active whisking were rare. The periods marked “I” and “II” are enlarged in Figure 1 – figure supplement 1A. **E.** To indicate the variability in whisker behavior, 100 trials of the same experiment were superimposed. The thick colored line indicates the median. The passive retraction is due to the air flow from the puffer and it is followed by an active protraction.

The following supplements are available for Figure 1:

Figure supplement 1 | Whisker movements are largely restricted to the period after the air-puff

Figure supplement 2 | Air-puffs induce reflexive whisker movements

Figure 2 | Anatomical distribution of Purkinje cell responses to whisker pad stimulation

A. Representative extracellular recording of a cerebellar Purkinje cell (PC) in an awake mouse showing multiple simple spikes (vertical deflections) and a single complex spike that is indicated by a blue dot above the trace. **B.** Scatter plot and histogram of complex spike firing around the moment of air-puff stimulation of the whisker pad (applied at 0.5 Hz) of the same PC. **C.** The latencies vs. the peak of the complex spike responses of all 118 PCs with a significant complex spike response. Note that a minority of the PCs showed relatively long latency times. **D.** Simple spike responses of the same PC showing a bi-phasic response: first inhibition, then facilitation. Note that the simple spike firing frequency of this PC at rest is about 60-70 Hz. **E.** Peak amplitudes and peak latency times of simple spike responses of all 127 PCs showing a significant simple spike response to whisker pad stimulation. As simple spike responses were often found to be bi-phasic, we represented the first phase with closed and the second phase with open symbols. Non-significant responses are omitted. **F.** Simplified scheme of the somatosensory pathways from the whisker pad to the PCs and of the motor pathways directing whisker movement. The information flows from the whisker pad via the trigeminal nuclei and the thalamus to the primary somatosensory (S1) and motor cortex (M1). S1 and M1 project to the inferior olive via the nuclei of the meso-diencephalic junction (MDJ) and to the pontine nuclei. Both the inferior olive and the pontine nuclei also receive direct inputs from the trigeminal nuclei. The mossy fibers (MF) from the pontine nuclei converge with direct trigeminal MF and those of the reticular formation on the cerebellar granule cells (GrC) that send parallel fibers (PF) to the PCs. The inferior olive provides climbing fibers (CF) that form extraordinarily strong synaptic connections with the PCs. Both the PFs and the CFs also drive feedforward inhibition to PCs via molecular layer interneurons (MLI). The GABAergic PCs provide the sole output of the cerebellar cortex that is directed to the cerebellar nuclei (CN). The CN sends the cerebellar output both upstream via the thalamus

back to the cerebral cortex and downstream to motor areas in the brainstem and spinal cord. The whisker pad muscles are under control of the facial nucleus which is mainly innervated via the reticular formation. Several feedback loops complement these connections. For references, see main text. **G.** For most of the PC recordings in this study, the anatomical locations were defined by a combination of surface photographs and electrolytic lesions made after completion of the recordings. An example of such a lesion in crus 1 is shown here in combination with a Nissl staining. SL = simple lobule. **H**. Heat map showing the anatomical distribution of the strength of the complex spike responses projected on the surface of crus 1 and crus 2. The locations of all 132 recorded PCs were attributed to a rectangular grid. The average complex spike response strength was calculated per grid position and averaged between each grid position and its neighbor. The grey lines indicate the borders to the cerebellar zones (see Figure 2 - figure supplement 2D). **I.** The same for the variation in the first phase of the simple spike responses. Note that for the simple spikes the blue colors indicate suppression of firing rather than the absence of a response.

The following supplements are available for Figure 2:

Figure supplement 1 | Diversity in Purkinje cell responses

Figure supplement 2 | Anatomy of the whisker region in the cerebellar hemispheres

Figure 3 | Large reflexive whisker protractions are preceded by complex spikes

A. Upon sorting the whisker traces based on the presence (violet) or absence (magenta) of a complex spike (CS) produced by a simultaneously recorded PC in the first 100 ms after stimulus onset, it is apparent that the trials with a complex spike tended to have a stronger protraction. **B.** This observation was confirmed in the population of PCs with a significant complex spike response to air-puff stimulation (n = 55). **C.** Averaged convolved peri-stimulus time histograms of complex spikes (*blue*) and the averaged difference in whisker position

(*purple*) between trials with and without complex spikes. Complex spikes precede the observed differences in movement. Shaded areas indicate s.d. (**A**) or SEM (**B** and **C**). **D.** Time intervals between the peak of the complex spike response and the moment of maximal difference in whisker position between trials with and without complex spikes, indicating that the complex spikes lead the whisker movement by approximately 60 ms. **E.** Changes in average whisker angle before stimulation (period a; see time bar in panel **B**), in maximal retraction (period b) and in maximal protraction (period c) between trials with and without a complex spike in the 100 ms after an air-puff. * $p > 0.05$; ** $p < 0.01$; *** $p < 0.001$ (Wilcoxon matched pairs tests (with Bonferroni correction for multiple comparisons in **E**)). See also Source Data file.

The following supplements are available for Figure 3:

Figure supplement 1 | Correlation between complex spike firing and whisker protraction especially strong in the D2 zone

Figure supplement 2 | Coherent complex spike firing is specifically enhanced by whisker pad stimulation

Figure 4 | Instantaneous simple spike firing correlates with whisker protraction during reflex

A. Changes in the instantaneous simple spike (SS) firing rate (convolved with a 6 ms Gaussian kernel; *blue*) correlate roughly with whisker movement (*purple*). This is illustrated with a representative recording of a PC. Vertical brown lines indicate the moments of air-puff stimulation to the (ipsilateral) whisker pad. The horizontal black line designates the interval expanded in **B**. Blue dots mark complex spikes. **C.** Correlation matrix showing a clear positive correlation of simple spike firing (blue trace at the bottom shows convolved peri-stimulus time histogram triggered on air-puff stimulation) and whisker protraction (red trace

at the left; indicated is the mean ± SEM of the whisker position) based on a trial-by-trial analysis. The correlation coefficient (R) over the dashed 45° line is shown at the bottom, together with the 99% confidence interval (*grey area*). These data correspond to the example PC shown in **A**-**B**. Averaged data from all 25 PCs that displayed a significant correlation between simple spike rate and whisker position is shown in **D**. **E.** Scatter plots with linear regression lines show a positive correlation between whisker protraction and instantaneous simple spike firing as illustrated here for the Purkinje cell represented in **C** (R = 0.517; $p < 0.001$; Pearson's correlation). Data are taken from the moment with the strongest correlation (150-160 ms after the onset of the air-puff for both parameters). **F.** For all PCs with a significant correlation between whisker angle and simple spike rate, this correlation turned out to be positive when evaluating 100 trials for each of the 25 Purkinje cells (R = 0.199; $p < 0.001$; Pearson's correlation). Shown is the linear regression line (*black*) and the 95% confidence intervals (*blue*). The experiments are normalized based upon their Z-score. Data are taken from the moment with the strongest correlation (120-130 ms (whiskers) vs. 140-150 ms (simple spikes)). Thus, increased simple spike firing correlates with whisker protraction. ** $p < 0.01$; *** $p < 0.001$.

The following supplement is available for Figure 4:

Figure supplement 1 | Simple spike firing is predominantly associated with protraction

Figure 5 | 4 Hz air-puff stimulation leads to acceleration of the simple spike response and to stronger protraction of the whiskers

A. Induction protocol: air-puff stimulation at 0.5 Hz is used to characterize the impact of a brief period (20 s) of 4 Hz air-puff stimulation. **B.** Stacked line plots showing the averaged whisker responses before (1st column) and after (2nd column) 4 Hz air-puff stimulation. The plots are sorted by the increase of the touch-induced whisker protraction (3rd column). Each

color depicts one mouse. Plots are normalized so that the most intense color represents the average of 16 mice. 4 Hz air-puff stimulation leads to a stronger touch-induced whisker protraction (4th column). Similar plots for complex spikes (**C**, showing little change) and simple spikes (**D**, showing a clear increase in firing, especially during the early phase of the response). For comparison, the averages are superimposed in **E** (for y-scaling and variations refer to **B**-**D**). Trial-by-trial analysis of 14 Purkinje cells before and after 4 Hz air-puff stimulation (cf. Figure 4C-D) highlighting the anticipation of simple spike firing (**F**). The x-axis is based upon the instantaneous simple spike firing frequency and the y-axis upon the whisker angle. The moment of maximal correlation between simple spike firing and whisker movement anticipated after induction, as can be seen by the change in position of the yellow spot between the correlation plots in the 1st and 2nd column (see also Figure 5 – figure supplement 1A-B). After induction, the maximal correlation implied a lead of the simple spikes, as illustrated for each PC in the graph of the 3rd column. Every arrow indicates the shift of the position of the maximal correlation between before and after induction. Overall, the difference in timing between the maximal correlation changed from around 0 ms pre-induction to an approximate lead of 20 ms of the simple spikes after induction (4th column). ** $p < 0.01$; *** $p < 0.001$. See also Table S2 and Source Data File.

The following supplements are available for Figure 5:

Figure supplement 1 | Simple spike response anticipates after 4 Hz air-puff stimulation

Figure supplement 2 | Purkinje cell responses during 4 Hz air-puff stimulation

Figure supplement 3 | Contralateral whisker pad stimulation induces stronger whisker protraction and stronger simple spike responses

Figure supplement 4 | Optogenetic stimulation of Purkinje cells increases whisker protraction following air-puff stimulation

Figure 6 | Complex spikes inhibit increased simple spike firing

A. Repeated sensory stimulation induced an increase in simple spike (SS) response to whisker pad stimulation (see Figure 5). This increase in simple spike responses was, however, not observed in all PCs: there was a clear negative correlation between the strength of the complex spike (CS) response and the potentiation of the simple spike response. Overall, the simple spike potentiation was larger in the PCs with a weak complex spike response than in those with a strong complex spike response (cf. Figure 2 – figure supplement 1). **B.** Heat map showing the anatomical distribution of the strength of the simple spike increase projected on the surface of crus 1 and crus 2. The 55 PCs were attributed to a rectangular grid. The average simple spike response strength was calculated per grid position and averaged between each grid position and its neighbor. The grey lines indicate the borders to the cerebellar zones (see Figure 2 - figure supplement 2D). **C.** Heat map of the distribution of PCs cells based upon the correlation of their simple spike rate and whisker position (cf. Figure 4D). Note that the strongest increase of simple spike responses after 4 Hz air-puff stimulation occurred in the region that also displayed the strongest correlation between instantaneous simple spike rate and whisker position. **D.** Example PSTHs of the simple spike response to whisker pad air-puff stimulation of representative PCs and how they changed over time, depicted as heat maps of the instantaneous simple spike frequency (**E**; see scale bar in **D**). The left column displays the data from a PC with a weak complex spike response, the right column of one with a strong complex spike response. The induction period is indicated with "4 Hz". **F.** The number of simple spikes following an air-puff stimulation increased in weakly responding Purkinje cells and this increase remained elevated until the end of the recording (at least 30 min). In contrast, this increase was not found in Purkinje cells with strong complex spike responses. * $p < 0.05$; ** $p < 0.01$; *** $p < 0.001$.

The following supplements are available for Figure 6:

Figure supplement 1 | Complex spike rates are negatively correlated with sensory-induced potentiation

Figure supplement 2 | 4 Hz air-puff stimulation enhances stereotypic whisker protraction for at least 30 minutes

Figure 7 | Expression of PP2B in Purkinje cells is required for increased protraction and simple spike firing following 4 Hz air-puff stimulation

A. Schematic representation of the principal pathways regulating bidirectional plasticity at the parallel fiber (PF) to Purkinje cell (PC) synapses. The direction of PF-PC plasticity depends on the intracellular Ca^{2+} concentration ($[Ca^{2+}]_i$) that is largely determined by climbing fiber (CF) activity. Following CF activity, $[Ca^{2+}]_i$ raises rapidly and activates a phosphorylation cascade involving α-Ca^{2+}/calmodulin-dependent protein kinase II (CaMKIIA) and several other proteins eventually leading to internalization of AMPA receptors and consequently to long-term depression (LTD). PF volleys in the absence of CF activity, on the other hand, result in a moderate increase in $[Ca^{2+}]_i$, activating a protein cascade involving protein phosphatase 2B (PP2B) that promotes the insertion of new AMPA receptors into the postsynaptic density, thereby leading to long-term potentiation (LTP) of the PF-PC synapse. GluA3 subunits are part of the postsynaptic AMPA receptors. **B.** Example of a representative mouse with the averaged whisker movements before and after theta sensory stimulation, showing a stronger protraction afterwards, as evidenced by the differences between post- and pre-induction compared to a bootstrap analysis on the normal variation in whisker movements (**C**; shade: 99% confidence interval). Variations in whisker protraction in L7-PP2B mutants did generally not exceed the expected variability (right). **D.** Stacked line plots of whisker

movement differences between post- and pre-induction for all mice highlighting the absence of increased touch-induced whisker protraction in L7-PP2B mutant mice. The plots are normalized so that the brightest line indicates the average per genotype (n = 16 WT and n = 13 L7-PP2B KO mice). **E.** The average maximal protraction before and after induction for each mouse confirms the increase in WT, but not in L7-PP2B mutant mice. The colored symbols indicate the average per genotype. **F.** In contrast to simple spike responses in WT mice, those in L7-PP2B KO mice could not be potentiated by our 4 Hz air-puff stimulation protocol. This effect was stable, also during longer recordings. For this analysis, we selected those with weak complex spike responses, as the PCs with a strong complex spike response did not show increased simple spike firing after 4 air-puff stimulation (see Figure 6A). * p < 0.05; ** p < 0.01; *** p < 0.001

The following supplement is available for Figure 7:

Figure supplement 1 | Also in L7-PP2B KO mice, complex spike rates are negatively correlated with sensory-induced potentiation

Figure 8 | Expression of AMPA receptor GluA3 subunits in Purkinje cells is required for increased protraction and simple spike firing following 4 Hz air-puff stimulation

A. Example of a representative L7-GluA3 mutant mouse with the averaged whisker movements before and after 4 Hz air-puff stimulation, showing similar degrees of protraction. **B.** Overall, 4 Hz air-puff stimulation did not result in stronger whisker protraction in L7-GluA3 mutant mice as observed in WT mice (see Figure 7). This is illustrated with a stacked line plot. **C.** Comparison of the average change in whisker angle over the 120 ms following the onset of the air-puff shows enhanced protraction in WT (n = 16), but not in LTP-deficient mice - neither in L7-PP2B (n = 13) nor in L7-GluA3 (n = 6) mutants, pointing towards a

central role for parallel fiber-to-Purkinje cell LTP for the enhanced protraction in WT mice following a brief period of 4 Hz air-puff stimulation. The horizontal lines indicate the medians and the 1st and 3rd quartiles. The lack of change in whisker protraction following 4 Hz air-puff stimulation was reflected in the lack of change in simple spike responses as illustrated in three representative PCs (cf. Figure 6D-E). On top are the peri-stimulus time histograms (**D**) followed by heat maps illustrating the instantaneous firing rate over time (**E**). The induction period is indicated with "4 Hz". F. Overall, WT PCs (n = 35) showed increased simple spike firing after 4 Hz stimulation, while those in L7-PP2B (n = 21) or L7-GluA3 (n = 13) mutant mice did not. For this analysis, we restricted ourselves to the PCs with weak complex spike responses as the PCs with strong complex spike responses did not show potentiation in the WT mice (see Figure 6A) and to the first 100 trials after induction. * $p < 0.05$; ** $p < 0.01$. See also Source Data File.

The following supplements are available for Figure 8:

Figure supplement 1 | Purkinje cell responses to whisker pad stimulation in L7-PP2B and L7-GluA3 mice

Figure supplement 2 | Before induction, touch-induced whisker protraction is not affected by L7-PP2B and L7-GluA3 mutations

Supplementary figure legends

Figure 1 – figure supplement 1 | Whisker movements are largely restricted to the period after the air-puff

A. During a prolonged period of 0.5 Hz whisker pad stimulation, in roughly half the trials the stereotypic whisker movement – passive retraction followed by a large active forward sweep – is followed by a prolonged period of more variable whisker movements. The traces show here the whisker movement (averaged over all trackable whiskers) during the two trials marked "I" and "II" in Figure 1D. **B.** Violin plots showing the amplitudes (difference between maximal retraction and maximal protraction in three 200 ms interval (relative to the start of the air-puff: -200 – 0 ms (Pre-stim), 0 – 200 ms (Stim) and 200 – 400 ms (Post-stim))) of individual trials of 16 mice (with approximately 100 trials per mouse). Horizontal lines represent 10^{th}, 25^{th}, 50^{th}, 75^{th} and 90^{th} percentiles. **C.** Fractions of trials with movements exceeding 10°. Asterisks indicate significantly different fractions of trials with movement. *** $p < 0.001$ ($\chi^2 = 1470.24$; 3x2 $\chi 2$ test).

Figure 1 – figure supplement 2 | Air-puffs induce reflexive whisker movements

A. Schematic drawing of the experimental layout. Air-puffs lasting 30 ms were delivered from three different locations. In addition, some air-puffs delivered ipsilaterally from the front were preceded by a brief air-puff (2 ms) 100 ms before the 30 ms air-puff to test for pre-pulse inhibition (PPI). The four stimulus conditions were applied in a random order. **B.** For each of the 9 mice tested, we calculated the average whisker response (always on the side with the two puffers) and represented these as summed line plots. The stacked line plots are scaled such that the brightest line (on top) depicts the average of all mice. The insets show the duration of the retraction (until the whiskers reached the baseline position again) comparing

the 2 ms and the 30 ms pulses (left) and the maximal protraction amplitudes upon the pre-pulse compared to the pulse (right). The passive retraction upon the short pre-pulse was less intense, but the consecutive protractions were of similar amplitude, indicating the absence of pre-pulse inhibition (p = 0.0078 and p = 0.4961, respectively; Wilcoxon matched-pairs tests; significance level = 0.025 after Bonferroni correction for multiple comparisons). **C.** Overlay of averaged ipsilateral whisker responses with shaded areas indicating ± SEM. The three ipsilateral conditions resulted in similar amounts of protraction. Note that the puff from the back did not cause a retraction preceding the protraction and that the pre-pulse did not affect the size of the protraction following the second air-puff. The brief pre-pulse induced a shorter retraction, but this had no effect on the protraction. Air-puffs to the contralateral whisker pad caused stronger protractions than the ipsilateral stimuli. **D.** The maximum retraction was largest when the air-puffer was in front of the ipsilateral whiskers. The shorter pre-pulse did cause a briefer retraction (see inset in **B**), but the amplitude was not significantly different from the retraction caused by the longer pulse (p = 0.268; Dunn's pair-wise post-hoc test after Friedman's two-way ANOVA; see Table S1). Puffing from the contralateral whiskers or the ipsilateral whiskers from the back caused the least retraction, indicating that the initial retraction is largely passive and caused by the air flow of the stimulator. **E.** The maximum protraction reached was similar for all conditions, except in case the contralateral whiskers were stimulated, which led to a stronger protraction on the ipsilateral side. n.s. $p > 0.05$; * $p < 0.05$; *** $p < 0.001$; *** $p < 0.001$. See also Source Data file.

Figure 2 - figure supplement 1 | Diversity in Purkinje cell responses

A. Single trial of a PC showing a relatively weak complex spike response to air-puff stimulation of the ipsilateral whisker pad. The dark blue dot indicates a complex spike. **B.** Raster plot and peri-stimulus time histogram (PSTH) of the complex spikes of the same

neuron as in **A**. Note that although the initial response is relatively weak, being present only in about 15% of the trials, this is still much more than could be expected based on the frequency during the inter-trial intervals. The dashed line indicates the average complex spike rate in between trials with the grey area representing ± 3 s.d.. **C.** The same for the simple spike response. This PC has a bimodal simple spike response, first a decrease and then an increase in simple spike activity. **D.** Based upon the complex spike response probability, defined as the peak of the complex spike response in the convolved PSTH, clustering the PCs into two clusters yielded the smallest Bayesian information criterion (BIC) value. **E.** The majority (66%) of the PCs could be classified as "weak responders" and the minority (34%) as "strong responders" (see pie diagram). This classification was obtained using a univariate Gaussian mixture model (blue and green lines, representing the two clusters). **F.** Comparison of the distribution of the observed complex spike responses and that expected by our model. **G.** The strength of the complex spike response and the first peak or trough (cf. panel **C**) in the simple spike (SS) response were not significantly correlated. Only the PCs with a very strong complex response tended to have a decrease in the simple spike response. **H.** The same applied for the second extremum of the simple spike response. For this later phase the complex spike and the simple spike responses were even less correlated.

Figure 2 - figure supplement 2 | Anatomy of the whisker region in the cerebellar hemispheres

A. PC locations could be retrieved by neural tracer injection (BDA 3000) after completion of the recording. In this example, tracer was found in the anterior interposed nucleus (IntA) (see arrow, area enlarged in **B**). SL = simple lobule; Med = medial nucleus; Lat = lateral nucleus; DLH = dorsolateral hump. Anterograde staining was observed in the cerebellar nuclei (**B**) and retrograde staining in the inferior olive (**C**) after a survival period of around 1 week. The

rectangle in the top micrograph of **C** indicates the area enlarged in the lower micrograph. **D.** A map is shown of the approximated locations of the recorded PCs. The names of the cerebellar zones are indicated. The response kinetics of complex spikes are shown as convolved peri-stimulus time histograms. In these traces, the left-most point represents the onset of the air-puff. Note that strong complex spike responses were observed in C3, D1 and D2 zones. DAO = dorsal accessory olive; PO = principal olive.

Figure 3 – figure supplement 1 | Correlation between complex spike firing and whisker protraction is especially strong in the D2 zone

A. There was no obvious correlation between the strength of the complex spike response of any given PC and the difference in touch-induced whisker protraction in trials with and without a complex spike. **B.** Indeed, and with the exception of the lateral most portion of crus 1, the predictive value of the occurrence of a complex spike was quite evenly distributed over crus 1 and crus 2. Together with the findings of **A**, this implies that the extent of stronger protraction in trials with a complex spike does not depend on the response characteristics of a PC. In other words, the predictive value of a complex spike is similar whether it originates from a weak or from a strong responder. However, as the PCs in the lateral zones display more complex spikes, their overall impact on whisker protraction is larger (**C**). Thus, complex firing in the D2 zone had the strongest predictive value for increased touch-induced whisker protraction.

Figure 3 – figure supplement 2 | Coherent complex spike firing is specifically enhanced by whisker pad stimulation

A. Field of view of a piece of crus 1 recorded using two-photon Ca^{2+} imaging in an awake mouse. The colored areas indicate 22 regions of interest, corresponding to PC dendrites. The

accompanying fluorescent traces show Ca^{2+} transients, which are most likely complex spikes (**B**; cf. Schultz et al., 2009). In the absence of tactile stimulation coherent activity of groups of PCs is rare. **C.** Following air-puff stimulation of the whisker pad (brown vertical lines), complex spike coherence occurs often as illustrated by five responsive PCs recorded simultaneously. **D.** Aggregate peri-stimulus time histogram of all PCs in the field of view shown in panel **A**. The colors represent the coherence of PC firing, defined as the fraction of PCs active during each frame of 40 ms. Complex spike coherence is relatively rare during inter-trial intervals, but strongly enhanced following air-puff stimulation. **E.** The same peri-stimulus histogram as in **D**, but with colors indicating the chance of occurrence of the level of coherence found based upon Poisson distribution of all complex spikes in this recording, emphasizing that coherence occurred more than expected, mainly during the sensory response. Indeed, during 1 Hz air-puff stimulation, complex spikes were observed to be produced by large ensembles. In the absence of tactile stimulation, ensemble sizes tended to be smaller (**F**). The data presented in panels **D**-**F** come from the field of view shown in panel **A**. **G.** There was a shift from complex spikes fired by a single or a few Purkinje cells towards complex spikes fired by larger ensembles when introducing air-puff stimulation. Presented are the median and the inter-quartile range of the differences between the two histograms as illustrated for an example experiment in panel **F** (n = 10). The increase in coherence directly after stimulation was highly significant (p = 0.001; Fr = 28.878; df = 9; Friedman's two-way ANOVA). * $p < 0.05$; ** $p < 0.01$, *** $p < 0.001$, **** $p < 0.0001$, ***** $p < 0.00001$.

Figure 4 - figure supplement 1 | Simple spike firing is predominantly associated with protraction

A. The average whisker response to air-puff stimulation (for reference, copied from Figure 4D). B. Overlaid plots of the correlation between whisker angle and instantaneous simple

spike frequency based on a trial-by-trial analysis of all 56 PCs measured in this way (see Figure 6). The correlation values are based upon the zero-lag correlation (thus along the "45° line" in Figure 4C,D). **C.** Stacked line plot of the 25 PCs with a significant correlation between whisker angle and simple spike firing. The cells are ordered based upon their correlation value and scaled so that the brightest line corresponds to the average. **D.** As in **C**, but now of the 31 PCs that did not show a significant correlation between their simple spike firing and the whisker position. Although the correlation is not significant when regarded per cell, overall there is a negative correlation between simple spike firing and whisker position. The darkest line corresponds to the average. **E.** Correlation matrix showing the correlation between whisker protraction (on the y axis) and instantaneous simple spike frequency (on the x-axis) of the 31 PCs that did not have a significant correlation between these two parameters. The heatmap represent the average R value for each bin (n = 31 PCs). The lookup table shows the color coding for the R values. **F.** Despite the lack of correlation at the single-cell level, at the population level these PCs correlated weakly but significantly in a negative manner (R = -0.067; $p < 0.001$; Pearson correlation), implying that they correlated more with retraction than with protraction. The black line indicates the linear regression line and the blue lines the 95% confidence interval. *** $p < 0.001$

Figure 5 – figure supplement 1 | Simple spike response anticipates after 4 Hz air-puff stimulation

A. Averaged zero-lag correlation (across the 45° line in Fig. 5F) of the instantaneous simple spike rate and whisker position before (magenta) and after (brown) 4 Hz air-puff stimulation, highlighting the faster achievement of the moment of maximal correlation after induction. This shift (again, along the 45° line) is further quantified and illustrated with a box plot (**B**). * $p < 0.05$. **C**. The slopes of the correlations between instantaneous simple spike firing rate and

the angle of the whisker are shown before and after 4 Hz air-puff stimulation for the 14 individual PCs that showed significant correlation. Despite the cells with the highest R correlation values were located in the lateral Crus 2, no clear difference was observed between the slope of the correlation of the PCs of Crus 1 (solid lines) and PCs of Crus 2 (dashed lines). **D**. No slopes change was observed after 4 Hz air-puff stimulation. This indicates that the plasticity induction did not change the amount of movement that corresponded to a certain number of spikes. See also Source Data file.

Figure 5 - figure supplement 2 | Purkinje cell responses during 4 Hz air-puff stimulation

A. Normalized stacked line plots showing the whisker movement in 16 mice during the pre-induction block (100 trials; left) and during the induction block (80 trials; right). The passive retractions, caused by the air flow, is largely intact, but the subsequent touch-induced whisker protraction is largely reduced during 4 Hz stimulation as compared to 0.5 Hz stimulation during the pre-induction block. **B.** Raster plots of the complex spike responses to whisker pad air-puff stimulation during the first 80 trials of a pre-induction block and during the 80 trials of the induction block with the accompanying peri-stimulus time histograms (**C**). **D.** Normalized stacked line plots show that the rate of complex spike responses is reduced upon a higher stimulation frequency (n = 55). **E-F.** The same for the simple spike response. **G.** Box plots showing the decreased whisker, complex spike peak response and simple spike modulation during the first 200 ms after puff onset. * $p < 0.05$; *** $p < 0.001$ (Wilcoxon matched-pairs test). See also Source Data File.

Figure 5 – figure supplement 3 | Contralateral whisker pad stimulation induces stronger whisker protraction and stronger simple spike responses

A. Whisker traces of a representative mouse following air-puff stimulation of the ipsilateral (left panel) and contralateral (right panel) whisker pad (see scheme in **B**). Despite a similar strength of stimulation, the protraction of the whiskers was larger upon contralateral stimulation (cf. Figure 1 – figure supplement 2). **C.** Stacked line plots of the averaged whisker traces of 9 mice with the difference between the contralateral and ipsilateral stimulation depicted in the third column. **D.** Complex spike responses, on the other hand, were more prominent upon ipsilateral stimulation. **E.** The observation that increased simple spike firing correlates to enhanced whisker protraction (cf. Figure 4) was confirmed under these experimental conditions. * $p < 0.05$; *** $p < 0.001$. See also Data Source File.

Figure 5 - figure supplement 4 | Optogenetic stimulation of Purkinje cells increases whisker protraction following air-puff stimulation

A. Air-puff stimulation of the whisker pad induces reflexive touch-induced whisker protraction. **B.** This protraction is enhanced when the sensory stimulus is paired with optogenetic stimulation of PCs. These two panels show whisker traces from a L7-Ai27 mouse that expresses ChR2 specifically in its PCs. An optic fiber with a diameter of 400 μm was placed on the surface of the cerebellum centrally at the fissure between crus 1 and crus 2 (**C**). Optogenetic stimulation of these mice results in increased simple spike firing. Stacked line plots of the whisker traces of 7 mice tested in this way following air-puff stimulation alone (**D**) and in combination with PC stimulation (**E**). **F.** The increased PC activity correlated with stronger protraction as evidenced by the differential traces. The inset shows a comparison of the maximal protraction (Protr.) under the two stimulus conditions; *** $p < 0.001$ (paired *t* test). See also Source Data File.

Figure 6 - figure supplement 1 | Complex spike rates are negatively correlated with sensory-induced potentiation

A. Scatter plots with linear regression lines between complex spike (CS) (left) and simple spike (SS) frequency (right) during the pre-induction (top) and the induction (bottom) period with the percentage of change in simple spike response between post- and pre-induction. The complex spike firing rate was negatively correlated with the change in simple spike responses in those PCs that had weak complex spike responses (see Figure 2 - figure supplement 1) – both during the pre-induction and during the induction interval. However, no such significant correlation was found in the strong complex spike responders. The simple spike rate did not have a significant correlation with simple spike responses. **B.** In contrast to the absolute firing rate, the difference in complex spike firing during the pre-induction versus the induction block did not show a clear correlation with changes in simple spike responsivity (left). Increased simple spike firing during the induction block, however, correlated well with increased sensory simple spike responses during the post-induction block. Thick lines indicate significant linear correlations ($p < 0.002$).

Figure 6 - figure supplement 2 | 4 Hz air-puff stimulation enhances reflexive whisker protraction for at least 30 minutes

A. The variability in whisker movements is illustrated by superimposing the average whisker angle during the 100 trials before 4 Hz air-puff stimulation. The thick line indicates the median. **B.** The first 100 trials after induction of the same experiment as in **A**, showing a clear increase in whisker protraction. Violin plots showing the amplitudes (differences between maximal retraction and maximal protraction in the indicated 200 ms intervals; see **G2**) of individual trials before (**C**) and after (**D**) induction. Obviously, the most prominent whisker movements were observed in the period between 0 and 200 ms after whisker pad air-puff

stimulation, as compared to the 200 ms intervals before and after thisperiod (n = 16 mice). Horizontal lines denote the 10th, 25th, 50th, 75th and 90th percentiles. Fractions of trials with movements exceeding 10° before (**E**) and after (**F**) induction. Especially the active protraction during the first 200 ms after the stimulus is clearly enhanced. Note that the panels **A**, **C** and **E** are the same as in Figure 1 – figure supplement 1 and are displayed here to illustrate the impact of 4 Hz stimulation on whisker movements. **G1.** Averaged whisker traces (ordered per 100 trials) of seven mice where video data were available for the whole recording, showing less retraction and more protraction after induction. For clarity, only the average of the last 100 trials pre-induction is plotted. Color codes as in panel **H**. **G2.** Differential traces show that whiskers remain further protracted, but that over time this became faster. **H.** 4 Hz air-puff stimulation caused increased whisker protraction during the whole recording (30 min). The switch from retraction to protraction (calculated as the time at which the whisker were back at the resting position after the initial retraction) remained faster throughout the recording (**I**). * $p < 0.05$; *** $p < 0.001$.

Figure 7 - figure supplement 1 | Also in L7-PP2B KO mice, complex spike rates are negatively correlated with sensory-induced potentiation

A. Scatter plots with linear regression lines between complex spike (CS) (left) and simple spike (SS) frequency (right) during the pre-induction (top) and the induction (bottom) period with the percentage of change in simple spike response between post- and pre-induction in L7-PP2B KO mice (see Figure 6 – figure supplement 1 for the results of the WT littermates). The complex spike firing rate was negatively correlated with the change in simple spike responses, in particular during the induction interval. The simple spike rate did not have a significant correlation with simple spike responses. **B.** In contrast to the absolute firing rate, the difference in complex spike firing during the pre-induction versus the induction block did

not show a clear correlation with changes in simple spike responsivity (left). In this mutant, a correlation between CS firing (during induction) and changes in simple sensitivity was still observed, possibly reflected the fact that parallel fiber LTD is still intact in these mice. Thick lines indicate significant linear correlations ($p < 0.002$).

Figure 8 - figure supplement 1 | Purkinje cell responses to whisker pad stimulation in L7-PP2B and L7-GluA3 mice

A. Example recordings of Purkinje cell activity in a wild-type (WT) (top), a L7-PP2B deficient (middle) and a L7-GluA3 deficient mouse (bottom). The timing of air-puffs to the whisker pad is indicated with light brown lines and that of the complex spikes with black dots above the traces. Compared to their WT littermates, L7-PP2B mice had a mildly reduced complex spike rate (**B**), as well as fewer simple spikes (**C**) that on top were fired more regularly (lower CV2; **D**). In contrast, the L7-GluA3 mice showed firing patterns that were more similar to their WT littermates. For clarity, the two WT groups are pooled for visualization, but statistics were performed between mutants and their respective control littermates. **E.** Complex spike responses to air-puff stimulation were quite similar in the three groups, although the mutants tended to have lower peak responses (**F**) with normal timing (**G**). **H.** Simple spike responses to air-puff stimulation were similar between WT and L7-GluA3 mice, but L7-PP2B mice showed more inhibition upon stimulation (**I**) with a longer latency (J). * $p < 0.05$; ** $p < 0.01$; *** $p < 0.001$. See also Table S3 and Source Data File.

Figure 8 - figure supplement 2 | Before induction, touch-induced whisker protraction is not affected by L7-PP2B and L7-GluA3 mutations

The maximal touch-induced whisker protraction is similar between wild-type (n = 16), L7-PP2B (n = 13) and L7-GluA3 (n = 6) mutant mice, indicating that the amplitude of the reflex

itself is not affected by any of the mutations involved. p = 0.860, F = 0.152, ANOVA. See also Source Data file.

Table S1 – Overview of statistical tests on whisker movements – belonging to Figure 1 – figure supplement 2

Table S2 – Overview of statistical tests – belonging to Figure 5.

Table S3 – Overview of statistical tests – belonging to Figure 8 – figure supplement 1.

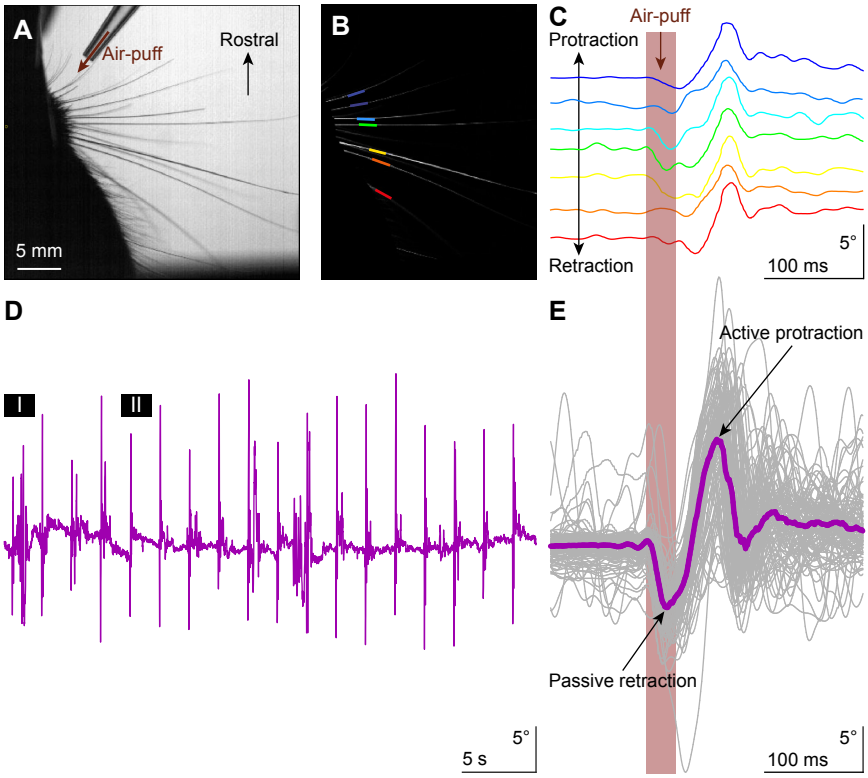

Figure 1 | Touch-induced whisker protraction
A brief (30 ms) air-puff to the whisker pad induces a reflexive protraction of all large mystacial whiskers. Our experiments were performed in awake, head-restrained mice that had all whiskers intact. **A.** Photograph showing a part of the mouse head with the large facial whiskers and the location and direction of the air-puffer (top). **B.** The large facial whiskers were recognized in high-speed videos (1 kHz full-frame rate) by a tracking algorithm and individual whiskers are color-coded. **C.** Air-puff stimulation triggered stereotypic whisker movements consisting of an initial passive backwards movement followed by active protraction. Deflection angles of individually tracked whiskers are denoted in distinct colors (same color scheme as in **B**). **D.** The mean whisker angle during 0.5 Hz air-puff stimulation of the whisker pad from a representative mouse. During approximately half the trials, the active protraction was only a single sweep; in the other traces multiple sweeps were observed. Prolonged periods of active whisking were rare. The periods marked “I” and “II” are enlarged in Figure 1 – figure supplement 1A. **E.** To indicate the variability in whisker behavior, 100 trials of the same experiment were superimposed. The thick colored line indicates the median. The passive retraction is due to the air flow from the puffer and is followed by an active protraction.

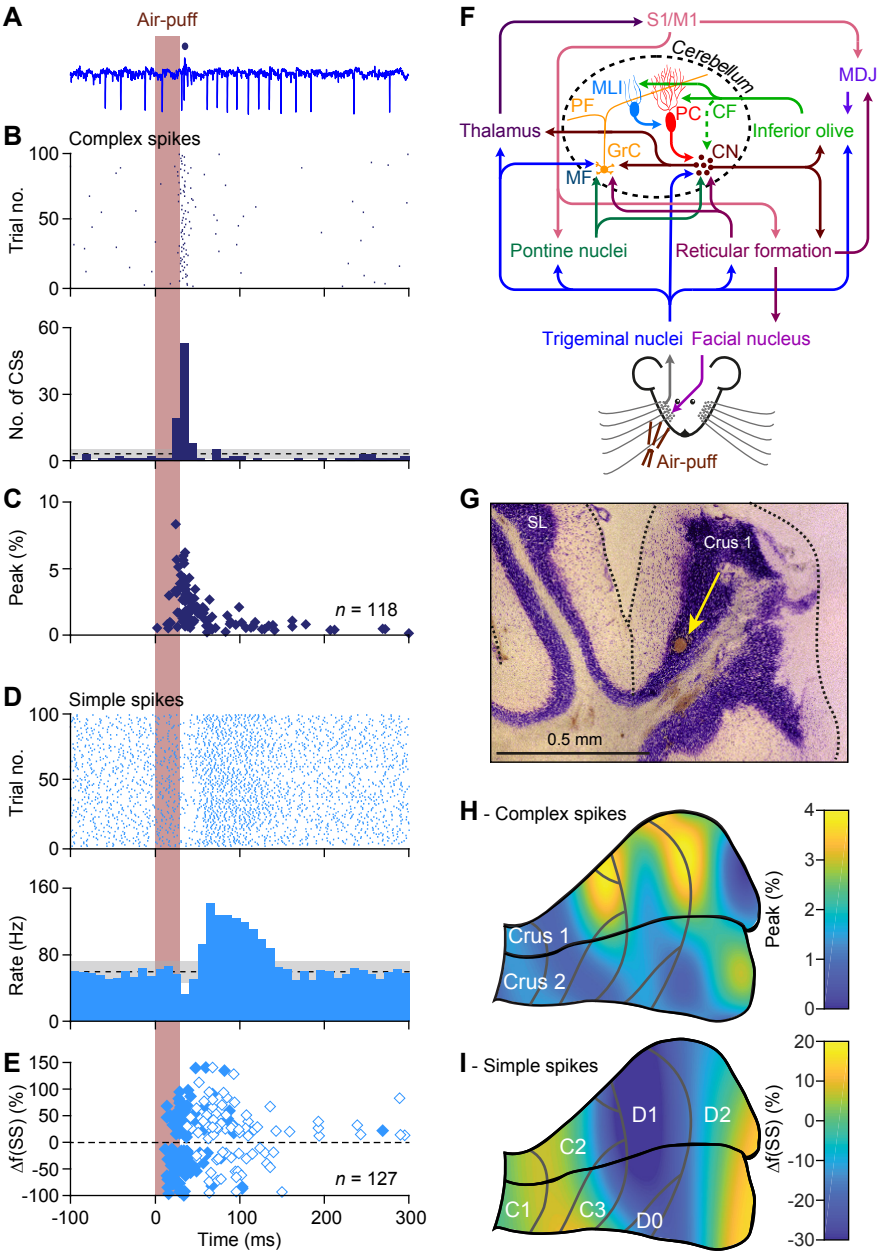

Figure 2 | Anatomical distribution of Purkinje cell responses to whisker pad stimulation

A. Representative extracellular recording of a cerebellar Purkinje cell (PC) in an awake mouse showing multiple simple spikes (vertical deflections) and a single complex spike that is indicated by a blue dot above the trace. **B.** Scatter plot and histogram of complex spike firing around the moment of air-puff stimulation of the whisker pad (applied at 0.5 Hz) of the same PC. **C.** The latencies vs. the peak of the complex spike responses of all 118 PCs with a significant complex spike response. Note that a minority of the PCs showed relatively long latency times. **D.** Simple spike responses of the same PC showing a bi-phasic response: first inhibition, then facilitation. Note that the simple spike firing frequency of this PC at rest is about 60-70 Hz. **E.** Peak amplitudes and peak latency times of simple spike responses of all 127 PCs showing a significant simple spike response to whisker pad stimulation. As simple spike responses were often found to be bi-phasic, we represented the first phase with closed and the second phase with open symbols. Non-significant responses are omitted. **F.** Simplified scheme of the somatosensory pathways from the whisker pad to the PCs and of the motor pathways directing whisker movement. The information flows from the whisker pad via the trigeminal nuclei and the thalamus to the primary somatosensory (S1) and motor cortex (M1). S1 and M1 project to the inferior olive via the nuclei of the meso-diencephalic junction (MDJ) and to the pontine nuclei. Both the inferior olive and the pontine nuclei also receive direct inputs from the trigeminal nuclei. The mossy fibers (MF) from the pontine nuclei converge with direct trigeminal MF and those of the reticular formation on the cerebellar granule cells (GrC) that send parallel fibers (PF) to the PCs. The inferior olive provides climbing fibers (CF) that form extraordinarily strong synaptic connections with the PCs. Both the PFs and the CFs also drive feedforward inhibition to PCs via molecular layer interneurons (MLI). The GABAergic PCs provide the sole output of the cerebellar cortex that is directed to the cerebellar nuclei (CN). The CN sends the cerebellar output both upstream via the thalamus back to the cerebral cortex and downstream to motor areas in the brainstem and spinal cord. The whisker pad muscles are under control of the facial nucleus which is mainly innervated via the reticular formation. Several feedback loops complement these connections. For references, see main text. **G.** For most of the PC recordings in this study, the anatomical locations were defined by a combination of surface photographs and electrolytic lesions made after completion of the recordings. An example of such a lesion in crus 1 is shown here in combination with a Nissl staining. SL = simple lobule. **H.** Heat map showing the anatomical distribution of the strength of the complex spike responses projected on the surface of crus 1 and crus 2. The locations of all 132 recorded PCs were attributed to a rectangular grid. The average complex spike response strength was calculated per grid position and averaged between each grid position and its neighbor. The grey lines indicate the borders to the cerebellar zones (see panel **I**). **I.** The same for the variation in the first phase of the simple spike responses. Note that for the simple spikes the blue colors indicate suppression of firing rather than the absence of a response.

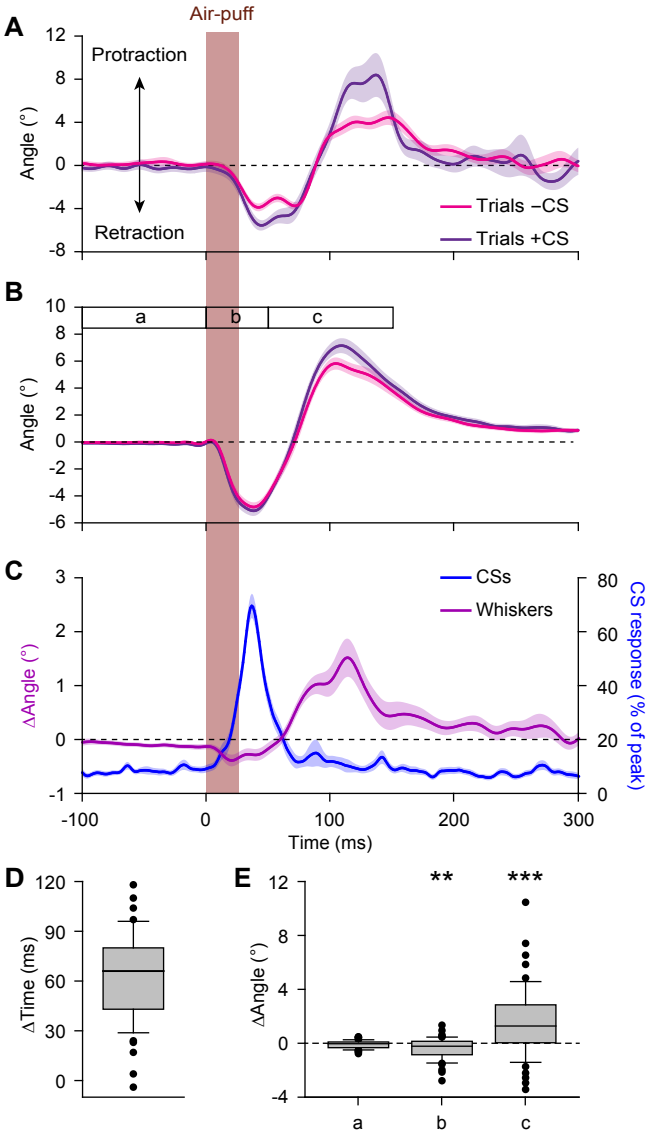

Figure 3 | Large reflexive whisker protractions are preceded by complex spikes

A. Upon sorting the whisker traces based on the presence (violet) or absence (magenta) of a complex spike (CS) produced by a simultaneously recorded PC in the first 100 ms after stimulus onset, it is apparent that the trials with a complex spike tended to have a stronger protraction. **B.** This observation was confirmed in the population of PCs with a significant complex spike response to air-puff stimulation (n = 55). **C.** Averaged convolved peri-stimulus time histograms of complex spikes (blue) and the averaged difference in whisker position (purple) between trials with and without complex spikes. Complex spikes precede the observed differences in movement. Shaded areas indicate s.d. (**A**) or SEM (**B** and **C**). **D.** Time intervals between the peak of the complex spike response and the moment of maximal difference in whisker position between trials with and without complex spikes, indicating that the complex spikes lead the whisker movement by approximately 60 ms. **E.** Changes in average whisker angle before stimulation (period a; see time bar in panel **B**), in maximal retraction (period b) and in maximal protraction (period c) between trials with and without a complex spike in the 100 ms after an air-puff. * $p > 0.05$; ** $p < 0.01$; *** $p < 0.001$ (Wilcoxon matched pairs tests (with Bonferroni correction for multiple comparisons in **E**)). See also Source Data file.

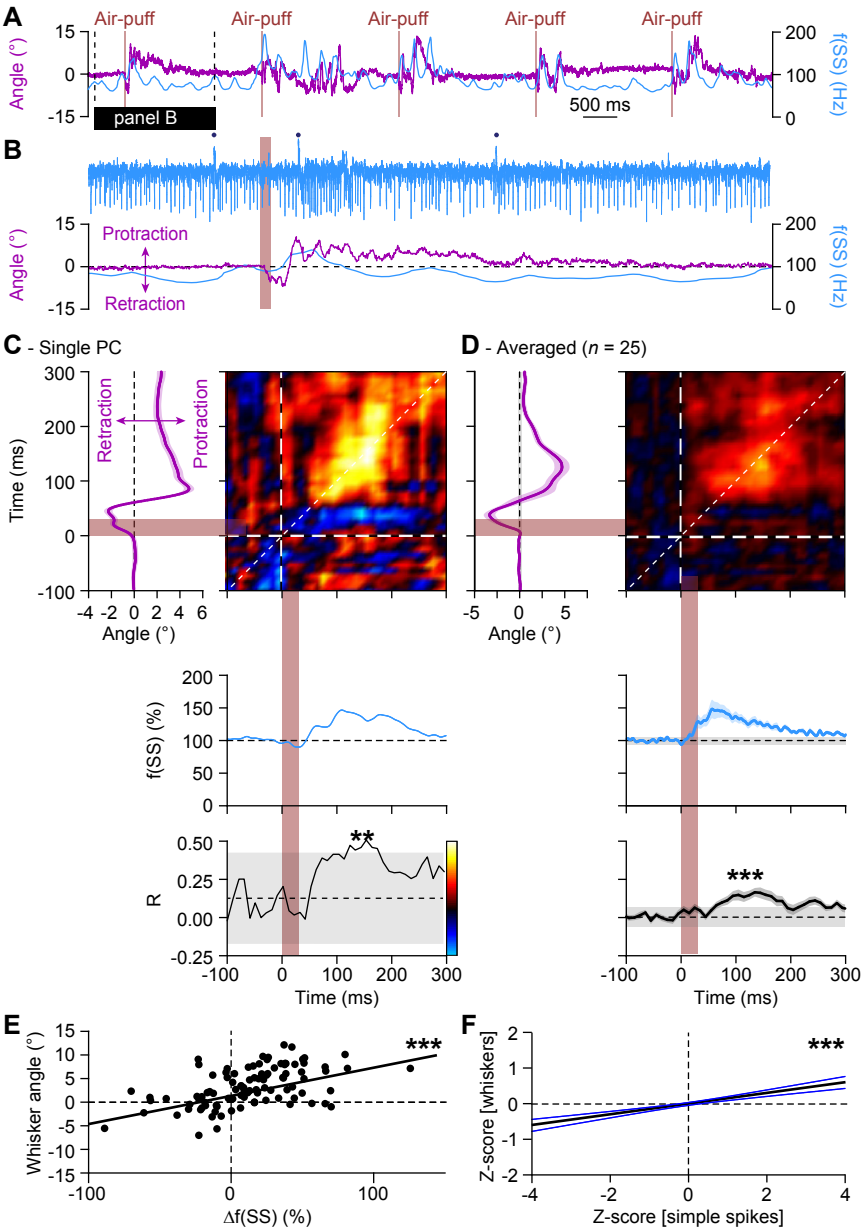

Figure 4 | Instantaneous simple spike firing correlates with whisker protraction during reflex

A. Changes in the instantaneous simple spike (SS) firing rate (convolved with a 6 ms Gaussian kernel; blue) correlate roughly with whisker movement (purple). This is illustrated with a representative recording of a PC. Vertical brown lines indicate the moments of air-puff stimulation to the (ipsilateral) whisker pad. The horizontal black line designates the interval expanded in **B**. Blue dots mark complex spikes. **C.** Correlation matrix showing a clear positive correlation of simple spike firing (blue trace at the bottom shows convolved peri-stimulus time histogram triggered on air-puff stimulation) and whisker protraction (red trace at the left; indicated is the mean ± SEM of the whisker position) based on a trial-by-trial analysis. The correlation coefficient (R) over the dashed 45° line is shown at the bottom, together with the 99% confidence interval (grey area). These data correspond to the example PC shown in **A**-**B**. Averaged data from all 25 PCs that displayed a significant correlation between simple spike rate and whisker position is shown in **D**. **E.** Scatter plots with linear regression lines show a positive correlation between whisker protraction and instantaneous simple spike firing as illustrated here for the Purkinje cell represented in **C** (R = 0.517; $p < 0.001$; Pearson's correlation). Data are taken from the moment with the strongest correlation (150-160 ms after the onset of the air-puff for both parameters). **F.** For all PCs with a significant correlation between whisker angle and simple spike rate, this correlation turned out to be positive when evaluating 100 trials for each of the 25 Purkinje cells (R = 0.199; $p < 0.001$; Pearson's correlation). Shown is the linear regression line (black) and the 95% confidence intervals (blue). The experiments are normalized based upon their Z-score. Data are taken from the moment with the strongest correlation (120-130 ms (whiskers) vs. 140-150 ms (simple spikes)). Thus, increased simple spike firing correlates with whisker protraction. ** $p < 0.01$; *** $p < 0.001$.

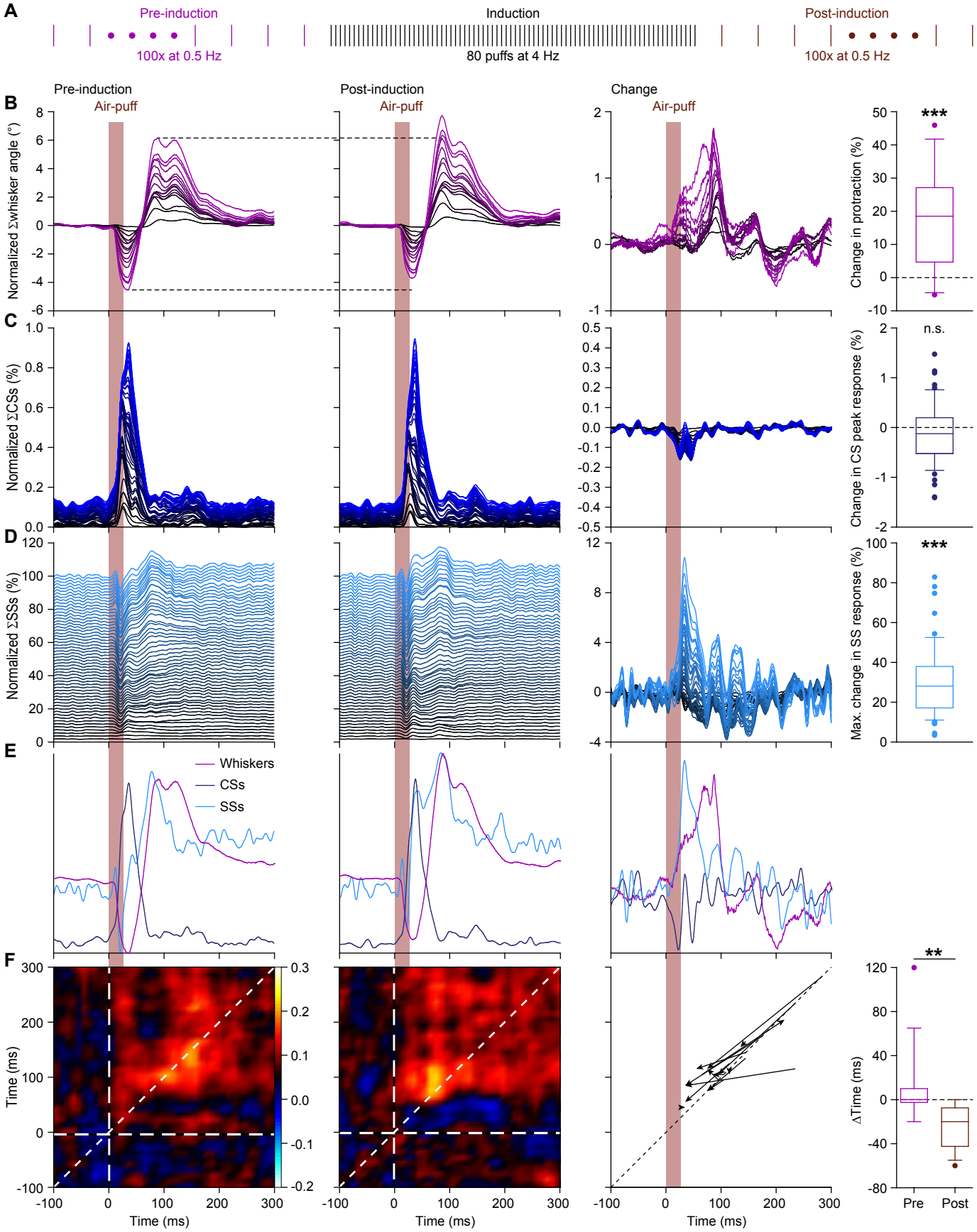

Figure 5 | 4 Hz air-puff stimulation leads to acceleration of the simple spike response and to stronger protraction of the whiskers

A. Induction protocol: air-puff stimulation at 0.5 Hz is used to characterize the impact of a brief period (20 s) of 4 Hz air-puff stimulation. **B.** Stacked line plots showing the averaged whisker responses before (1st column) and after (2nd column) 4 Hz air-puff stimulation. The plots are sorted by the increase of the touch-induced whisker protraction (3rd column). Each color depicts one mouse. Plots are normalized so that the most intense color represents the average of 16 mice. 4 Hz air-puff stimulation leads to a stronger touch-induced whisker protraction (4th column). Similar plots for complex spikes (**C**, showing little change) and simple spikes (**D**, showing a clear increase in firing, especially during the early phase of the response). For comparison, the averages are superimposed in **E** (for y-scaling and variations refer to **B**-**D**). Trial-by-trial analysis of 14 Purkinje cells before and after 4 Hz air-puff stimulation (cf. Figure 4C-D) highlighting the anticipation of simple spike firing (**F**). The x-axis is based upon the instantaneous simple spike firing frequency and the y-axis upon the whisker angle. The moment of maximal correlation between simple spike firing and whisker movement anticipated after induction, as can be seen by the change in position of the yellow spot between the correlation plots in the 1st and 2nd column (see also Figure 5 – figure supplement 1A-B). After induction, the maximal correlation implied a lead of the simple spikes, as illustrated for each PC in the graph of the 3rd column. Every arrow indicates the shift of the position of the maximal correlation between before and after induction. Overall, the difference in timing between the maximal correlation changed from around 0 ms pre-induction to an approximate lead of 20 ms of the simple spikes after induction (4th column). ** $p < 0.01$; *** $p < 0.001$. See also Table S2 and Source Data File.

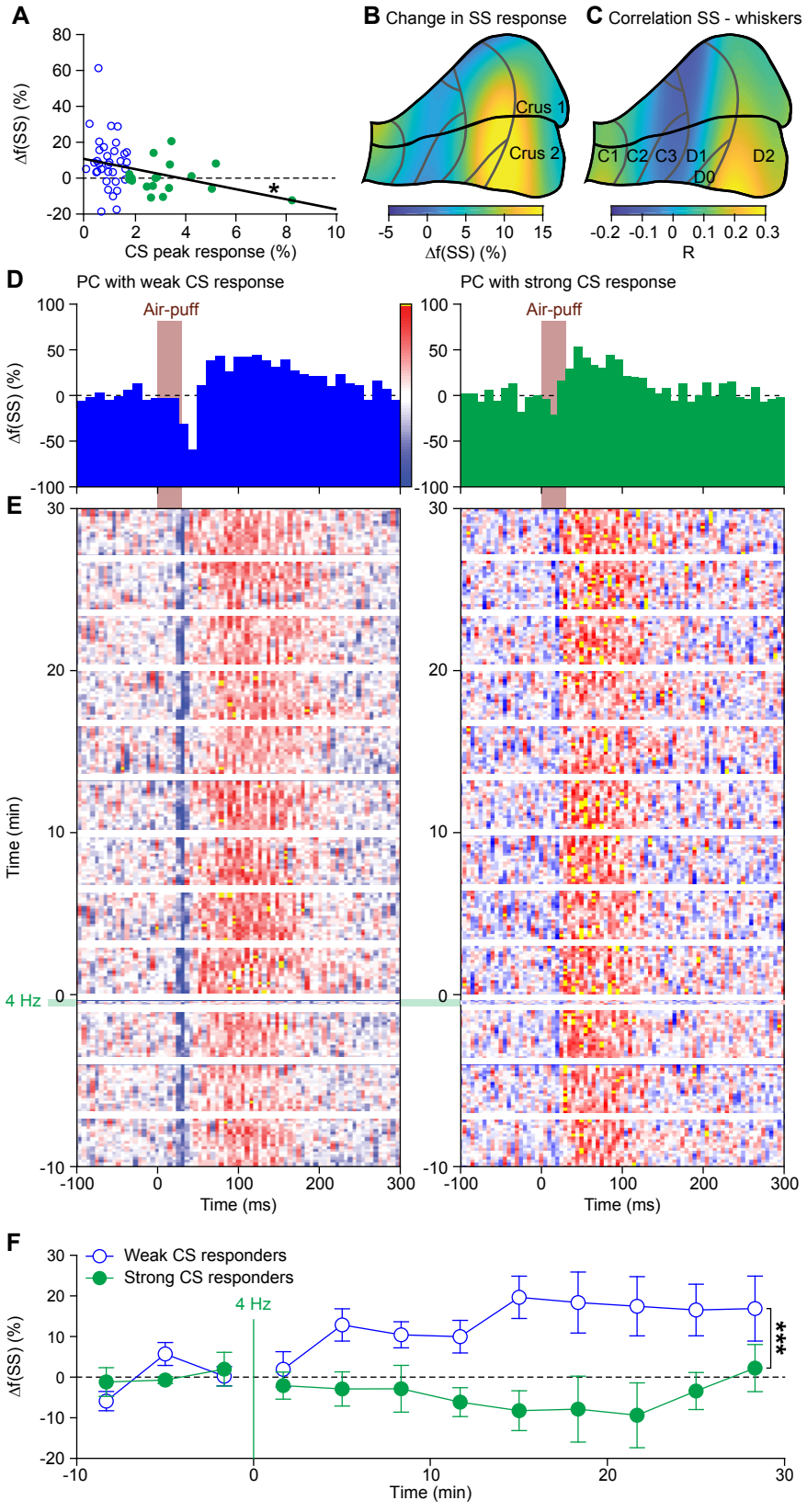

Figure 6 | Complex spikes inhibit increased simple spike firing
A. Repeated sensory stimulation induced an increase in simple spike (SS) response to whisker pad stimulation (see Figure 5). This increase in simple spike responses was, however, not observed in all PCs: there was a clear negative correlation between the strength of the complex spike (CS) response and the potentiation of the simple spike response. Overall, the simple spike potentiation was larger in the PCs with a weak complex spike response than in those with a strong complex spike response (cf. Figure 2 – figure supplement 1). **B.** Heat map showing the anatomical distribution of the strength of the simple spike increase projected on the surface of crus 1 and crus 2. The 55 PCs were attributed to a rectangular grid. The average simple spike response strength was calculated per grid position and averaged between each grid position and its neighbor. The grey lines indicate the borders to the cerebellar zones (see Figure 2I). **C.** Heat map of the distribution of PCs cells based upon the correlation of their simple spike rate and whisker position (cf. Figure 4D). Note that the strongest increase of simple spike responses after 4 Hz air-puff stimulation occurred in the region that also displayed the strongest correlation between instantaneous simple spike rate and whisker position. **D.** Example PSTHs of the simple spike response to whisker pad air-puff stimulation of representative PCs and how they changed over time, depicted as heat maps of the instantaneous simple spike frequency (**E**; see scale bar in **D**). The left column displays the data from a PC with a weak complex spike response, the right column of one with a strong complex spike response. The induction period is indicated with "4 Hz". **F.** The number of simple spikes following an air-puff stimulation increased in weakly responding Purkinje cells and this increase remained elevated until the end of the recording (at least 30 min). In contrast, this increase was not found in PCs with strong complex spike responses. * $p < 0.05$; ** $p < 0.01$; *** $p < 0.001$.

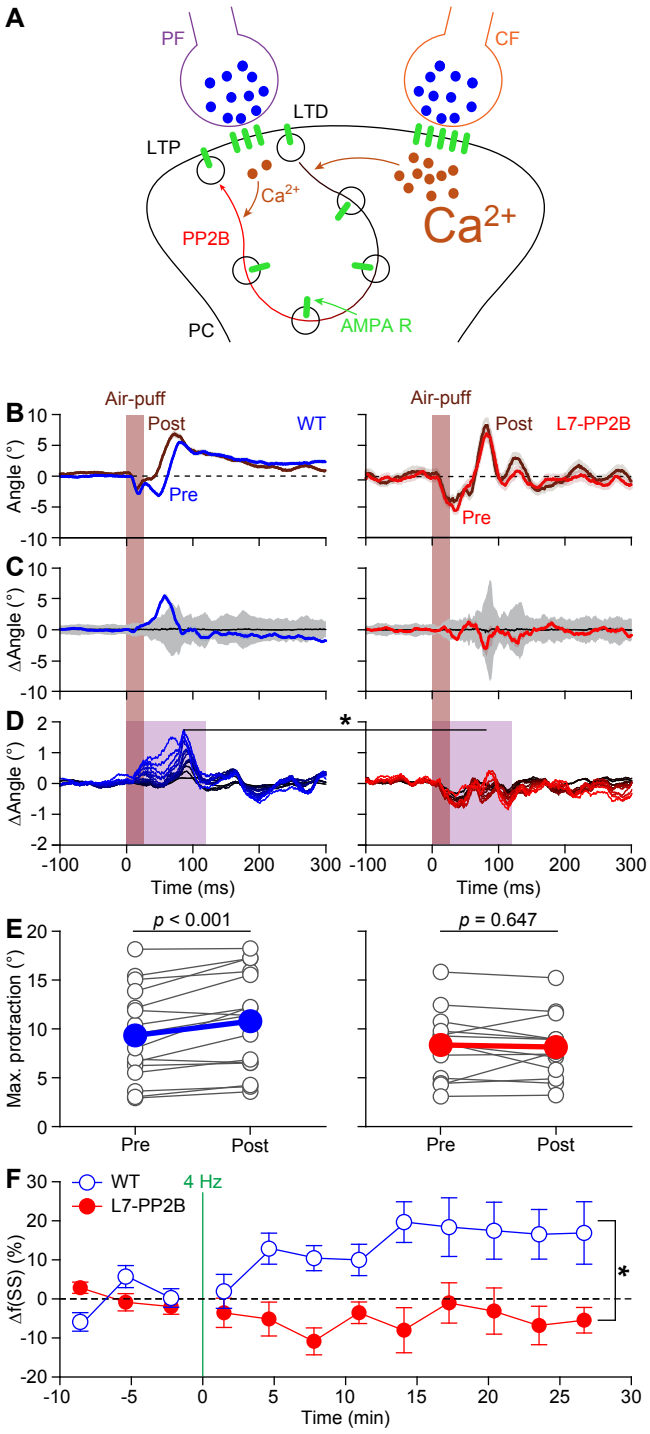

Figure 7 | Expression of PP2B in Purkinje cells is required for increased protraction and simple spike firing following 4 Hz air-puff stimulation
A. Schematic representation of the principal pathways regulating bidirectional plasticity at the parallel fiber (PF) to Purkinje cell (PC) synapses. The direction of PF-PC plasticity depends on the intracellular Ca^{2+} concentration ($[Ca^{2+}]_i$) that is largely determined by climbing fiber (CF) activity. Following CF activity, $[Ca^{2+}]_i$ raises rapidly and activates a phosphorylation cascade involving α-Ca^{2+}/calmodulin-dependent protein kinase II (CaMKIIA) and several other proteins eventually leading to internalization of AMPA receptors and consequently to long-term depression (LTD). PF volleys in the absence of CF activity, on the other hand, result in a moderate increase in $[Ca^{2+}]_i$, activating a protein cascade involving protein phosphatase 2B (PP2B) that promotes the insertion of new AMPA receptors into the postsynaptic density, thereby leading to long-term potentiation (LTP) of the PF-PC synapse. GluA3 subunits are part of the postsynaptic AMPA receptors. **B.** Example of a representative mouse with the averaged whisker movements before and after theta sensory stimulation, showing a stronger protraction afterwards, as evidenced by the differences between post- and pre-induction compared to a bootstrap analysis on the normal variation in whisker movements (**C**; shade: 99% confidence interval). Variations in whisker protraction in L7-PP2B mutants did generally not exceed the expected variability (right). **D.** Stacked line plots of whisker movement differences between post- and pre-induction for all mice highlighting the absence of increased touch-induced whisker protraction in L7-PP2B mutant mice. The plots are normalized so that the brightest line indicates the average per genotype (n = 16 WT and n = 13 L7-PP2B KO mice). **E.** The average maximal protraction before and after induction for each mouse confirms the increase in WT, but not in L7-PP2B mutant mice. The colored symbols indicate the average per genotype. **F.** In contrast to simple spike responses in WT mice, those in L7-PP2B KO mice could not be potentiated by our 4 Hz air-puff stimulation protocol. This effect was stable, also during longer recordings. For this analysis, we selected those with weak complex spike responses, as the PCs with a strong complex spike response did not show increased simple spike firing after 4 air-puff stimulation (see Figure 6A). * $p < 0.05$; ** $p < 0.01$; *** $p < 0.001$

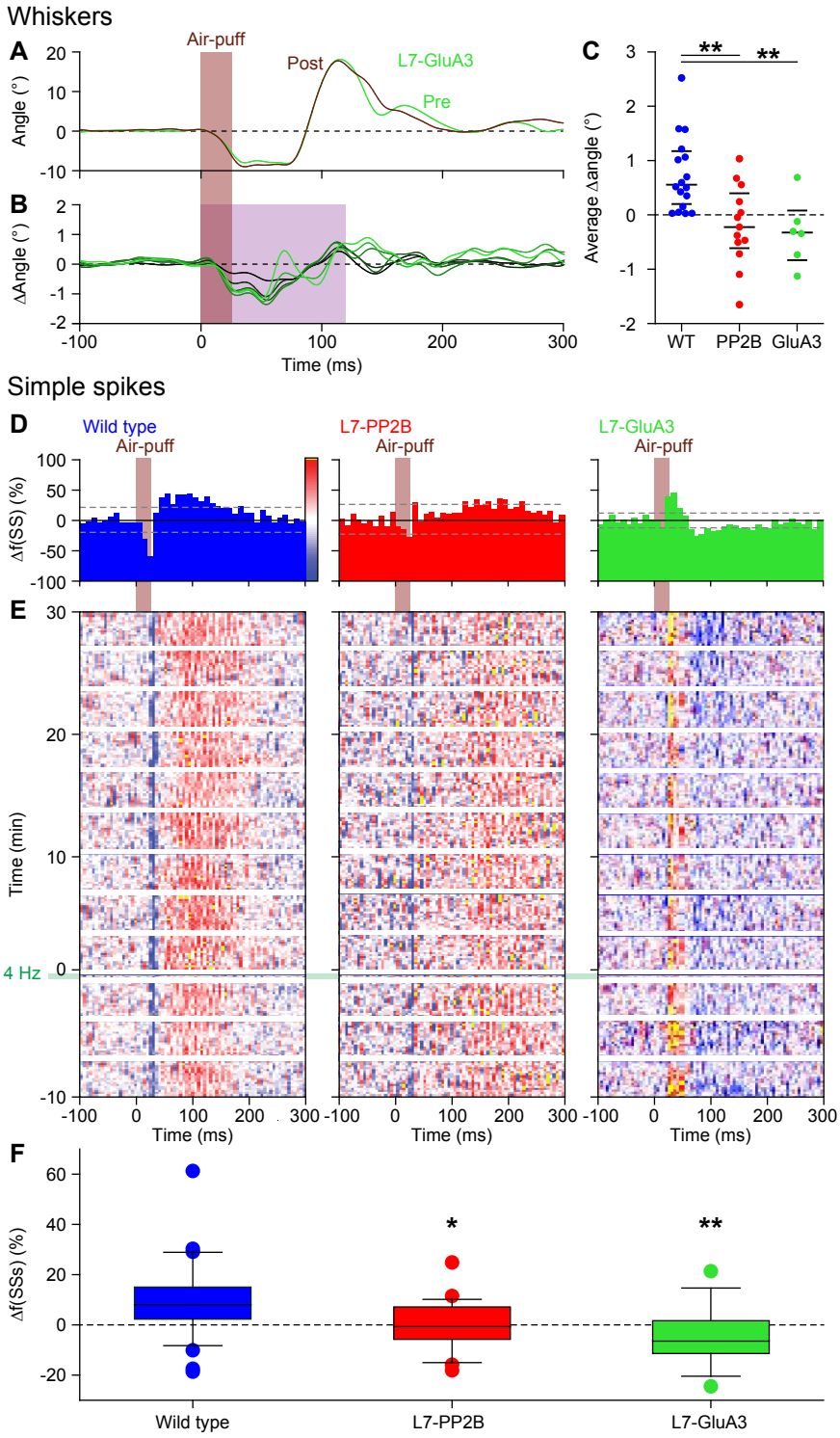

Figure 8 | Expression of AMPA receptor GluA3 subunits in Purkinje cells is required for increased protraction and simple spike firing following 4 Hz air-puff stimulation

A. Example of a representative L7-GluA3 mutant mouse with the averaged whisker movements before and after 4 Hz air-puff stimulation, showing similar degrees of protraction. **B.** Overall, 4 Hz air-puff stimulation did not result in stronger whisker protraction in L7-GluA3 mutant mice as observed in WT mice (see Figure 7). This is illustrated with a stacked line plot. **C.** Comparison of the average change in whisker angle over the 120 ms following the onset of the air-puff shows enhanced protraction in WT (n = 16), but not in LTP-deficient mice - neither in L7-PP2B (n = 13) nor in L7-GluA3 (n = 6) mutants, pointing towards a central role for parallel fiber-to-Purkinje cell LTP for the enhanced protraction in WT mice following a brief period of 4 Hz air-puff stimulation. The horizontal lines indicate the medians and the 1st and 3rd quartiles. The lack of change in whisker protraction following 4 Hz air-puff stimulation was reflected in the lack of change in simple spike responses as illustrated in three representative PCs (cf. Figure 6D-E). On top are the peri-stimulus time histograms (D) followed by heat maps illustrating the instantaneous firing rate over time (E). The induction period is indicated with "4 Hz". **F.** Overall, WT PCs (n = 35) showed increased simple spike firing after 4 Hz stimulation, while those in L7-PP2B (n = 21) or L7-GluA3 (n = 13) mutant mice did not. For this analysis, we restricted ourselves to the PCs with weak complex spike responses as the PCs with strong complex spike responses did not show potentiation in the WT mice (see Figure 6A) and to the first 100 trials after induction. * p < 0.05; ** p < 0.01. See also Source Data File.